Applied Thermal Engineering 212 (2022) 118533

Contents lists available at ScienceDirect

Applied Thermal Engineering

journal homepage: www.elsevier.com/locate/apthermeng

Research Paper

Thermal response analysis and parameter prediction of additively manufactured polymers

Navid Moslemi [a], Behzad. Abdi [b,*], Soheil Gohari [c], Izman Sudin [a], E. Atashpaz-Gargari [d], Norizah Redzuan [a], Amran Ayob [a], Colin Burvill [c], Meini Su [b], Farid Arya [e]

[a] School of Mechanical Engineering, Universiti Teknologi Malaysia (UTM), Skudai, 81310, Johor Bahru, Johor, Malaysia
[b] Department of Mechanical, Aerospace and Civil Engineering, Pariser Building, The University of Manchester, Manchester, United Kingdom
[c] Department of Mechanical Engineering, The University of Melbourne, Parkville, VIC, 3010, Australia
[d] Department of Engineering and Computing, National University, 11255 N Torrey Pines Rd, San Diego, CA 92037, United States
[e] Buckinghamshire New University, High Wycombe Campus, Queen Alexandra Road, High Wycombe, Buckinghamshire, United Kingdom

ARTICLE INFO

Keywords:
Finite element analysis
Artificial Neural Network
Polymers
Additive manufacturing
3D printing

ABSTRACT

Fused Deposition Modelling (FDM), is an additive manufacturing technology where polymers are extruded using appropriate processing parameters to achieve suitable bonding while ensuring that overheating does not occur. Among processing parameters, polymer inlet temperature, nozzle size, extrusion speed, and air cooling speed are significantly effect on the extrusion process at the distance between the build plate and the nozzle tip (standoff region). This study aims to evaluate the influences of the processing parameters on the thermal behavior and phase change zone of Polyamide 12 (PA12) and Acrylonitrile Butadiene Styrene (ABS) polymers at standoff region. A nonlinear three-dimensional (3D) finite element (FE) model was developed by implementing an apparent heat capacity model using the Heat Transfer Module in COMSOL® Multiphysics software. FE results in the standoff region were validated by experimental tests, concerning various nozzle sizes and extrusion speed. The validated numerical results demonstrated that there is a complex correlation between processing parameters and thermal behaviors such as phase change and temperature distribution in the standoff region. The FE results were then employed in training an artificial neural network (ANN). A well-established compromise between the trained ANN and the FE results demonstrates that the trained ANN can be employed in the prediction of further thermal and glass transition behavior using subsequent processing parameters.

1. Introduction

Three-dimensional (3D) printing technologies such as Fused Deposition Modelling (FDM), selective laser sintering and, more generally, additive manufacturing (AM) are of interest to researchers over the last few decades [1–3]. Unlike subtractive manufacturing technologies, additive manufacturing methods create 3D parts directly from 3D CAD models by adding melted polymer material layer by layer. Subtractive manufacturing methods typically use fabrication equipment such as cutting tools, fixtures and jigs [4]. In recent years, 3D printing techniques have become popular manufacturing processes and have been recognized as contributing to the 'third industrial revolution' [5–10].

For small product quantities, FDM technology is significantly low-cost and is efficient in terms of material, waste, energy and production time. Hence, FDM is one of the most popular additive manufacturing techniques and is extensively used in automotive, aerospace, medical, education and civil engineering industries [11–15]. In FDM, a feeder introduces a polymer filament into a heating block, where it is melted to a temperature higher than its glass transition temperature. Then, the molten polymer is extruded, cooled, and solidified onto the build plate layer by layer to form a 3D model. This method offers relatively poor accuracy with inferior surface quality when compared to models printed using other manufacturing techniques in the AM category [16]. In polymer 3D printing techniques such as FDM, wrapping, shrinkage, dimensional accuracy, and adhesion of printed material to the build plate are primarily influenced by thermal factors such as extrusion

* Corresponding author.
E-mail addresses: moslemi.navid@utm.my (N. Moslemi), behzad.abdi@manchester.ac.uk (Behzad. Abdi), soheil.gohari@unimelb.edu.au (S. Gohari), Izman@utm.my (I. Sudin), egargari@nu.edu (E. Atashpaz-Gargari), norizah@utm.my (N. Redzuan), amran@utm.my (A. Ayob), colb@unimelb.edu.au (C. Burvill), meini.su@manchester.ac.uk (M. Su), farid.arya@bucks.ac.uk (F. Arya).

https://doi.org/10.1016/j.applthermaleng.2022.118533
Received 23 November 2021; Received in revised form 8 April 2022; Accepted 13 April 2022
Available online 30 April 2022

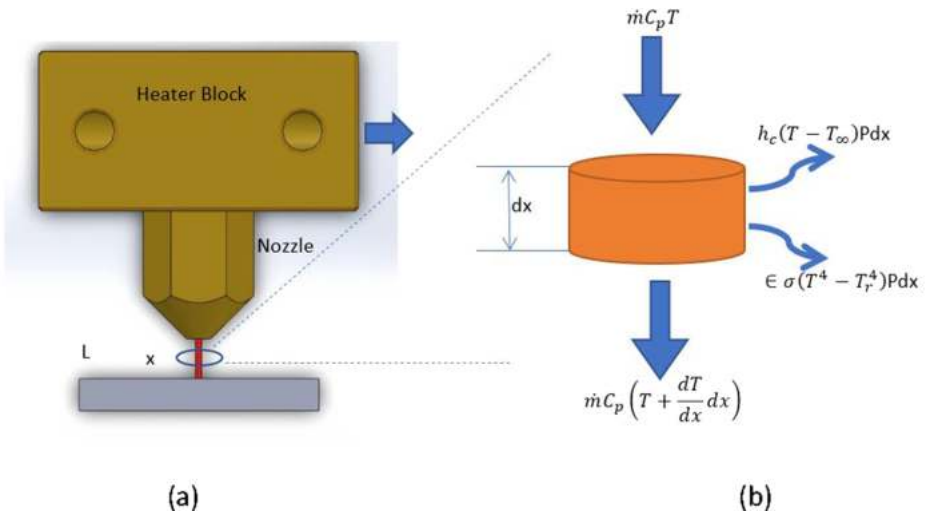

Fig. 1. (a) The schematic of the extrusion system in FDM process, (b) heat transfer in an element of the molten polymer within the standoff region of length dx.

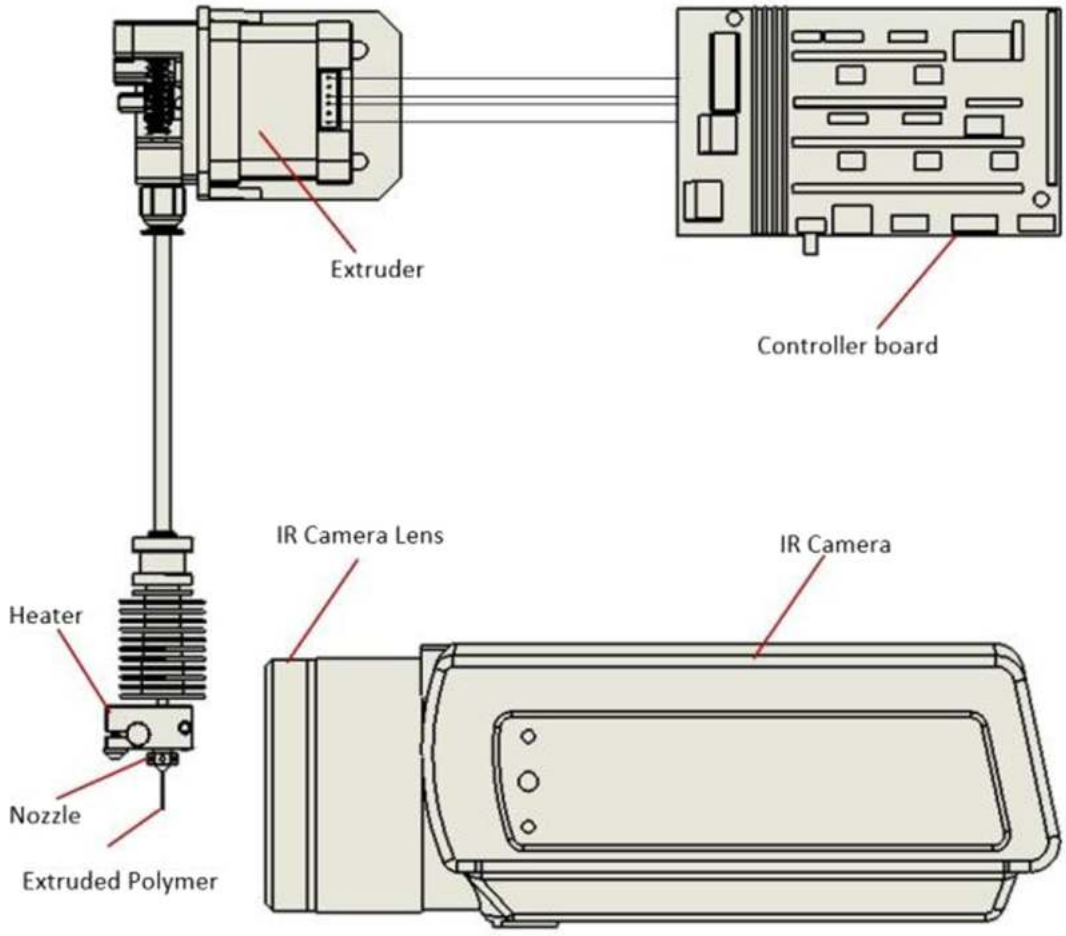

Fig. 2. A schematic of designed extrusion system and infrared thermal camera.

temperature, cooling rate, and melting temperature [17]. One solution to these temperature related issues is to determine best processing parameter values and then to calibrate the FDM to these processing parameters [18–21]. In FDM, the processing parameters include: layer thickness, build orientation, raster angle, air distance, extrusion temperature, print speed, infill pattern, nozzle diameter, raster width, and air-cooling rate influence on the mechanical properties and the final quality of the deposited parts [18,22–25]. In other words, the quality of the 3D printed products in terms of the thermal and mechanical properties are depended of the quality of the bonding between the lines and layers which can be controlled by adopting optimized parameters. Therefore, precise setting of processing parameters is critical to achieving best FDM printing performance [7,26].

In the extrusion process (Fig. 1), the molten polymer at a certain

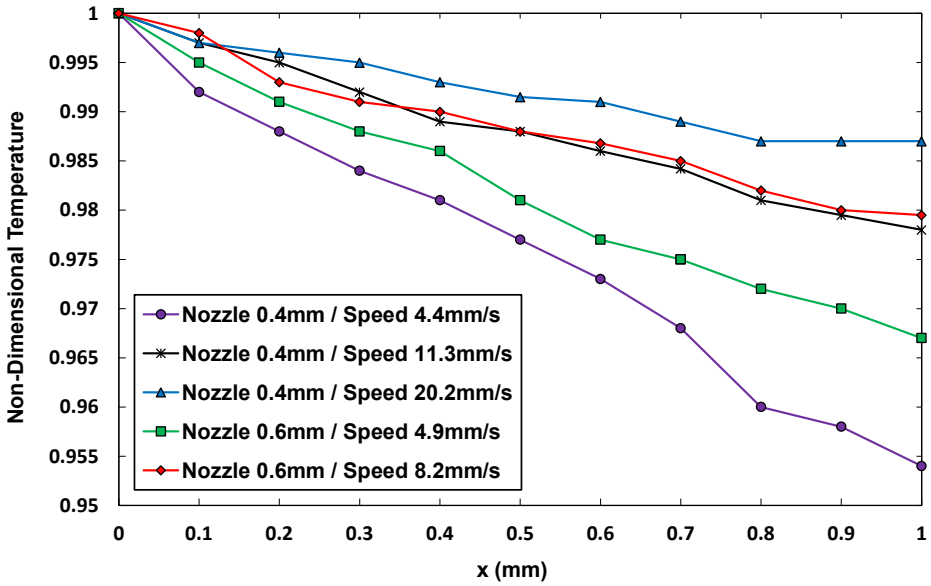

Fig. 3. The experimental results of temperature distribution of extruded ABS polymer at the distance between the nozzle tip and build plate.

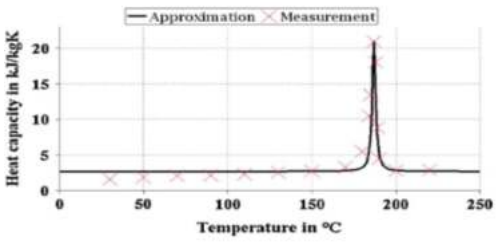

(a) Temperature dependent heat capacity.

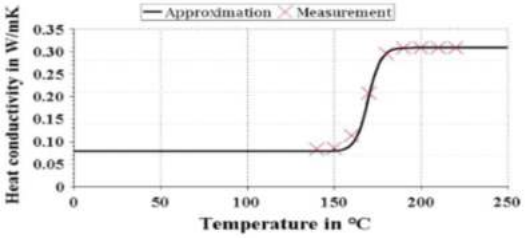

(b) Temperature dependent heat conductivity.

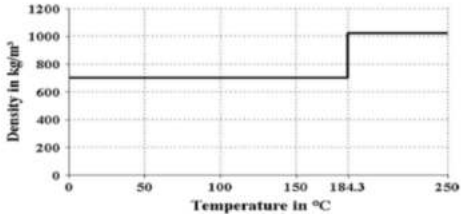

(c) Temperature dependent density.

Fig. 4. The temperature-dependent properties of PA12 polymer [70].

Table 1
The thermal conductivity, density and specific heat capacity of PA12 and ABS polymer in both glassy and rubbery states [63]

Thermal properties	Glassy state	Rubbery state	Unit
		PA12	
Thermal conductivity	0.078	0.32	$W/(m.K)$
density	710	1060	kg/m^3
Heat capacity	2095	2215	$J/(kg.K)$
	ABS		
Thermal conductivity	0.3	0.2	$W/(m.K)$
density	1050	970	kg/m^3
Heat capacity	1200	1708	$J/(kg.K)$

temperature is extruded from the nozzle tip and is then laid down over the build plate. Within the process, three heat transfer processes occur: in the nozzle, the distance between the nozzle tip and the build plate (standoff region), and at the build plate. These heat transfer processes affect the mechanical properties of the deposited part [27]. Despite typically being a short distance, the temperature distribution of the extruded polymer in the standoff region plays an important role in the process due to the associated unconstrained thermal gradients. Processing parameters play a significant role in identifying the thermal behavior of polymer in the standoff region.

Several research studies have been conducted to evaluate the heat transfer process in the distance between the nozzle tip and build plate using analytical, numerical, and experimental investigations [17,28–30].

Heat transfer plays a significant role in the melting and solidification of the polymer during the printing process. Controlling the heat transfer

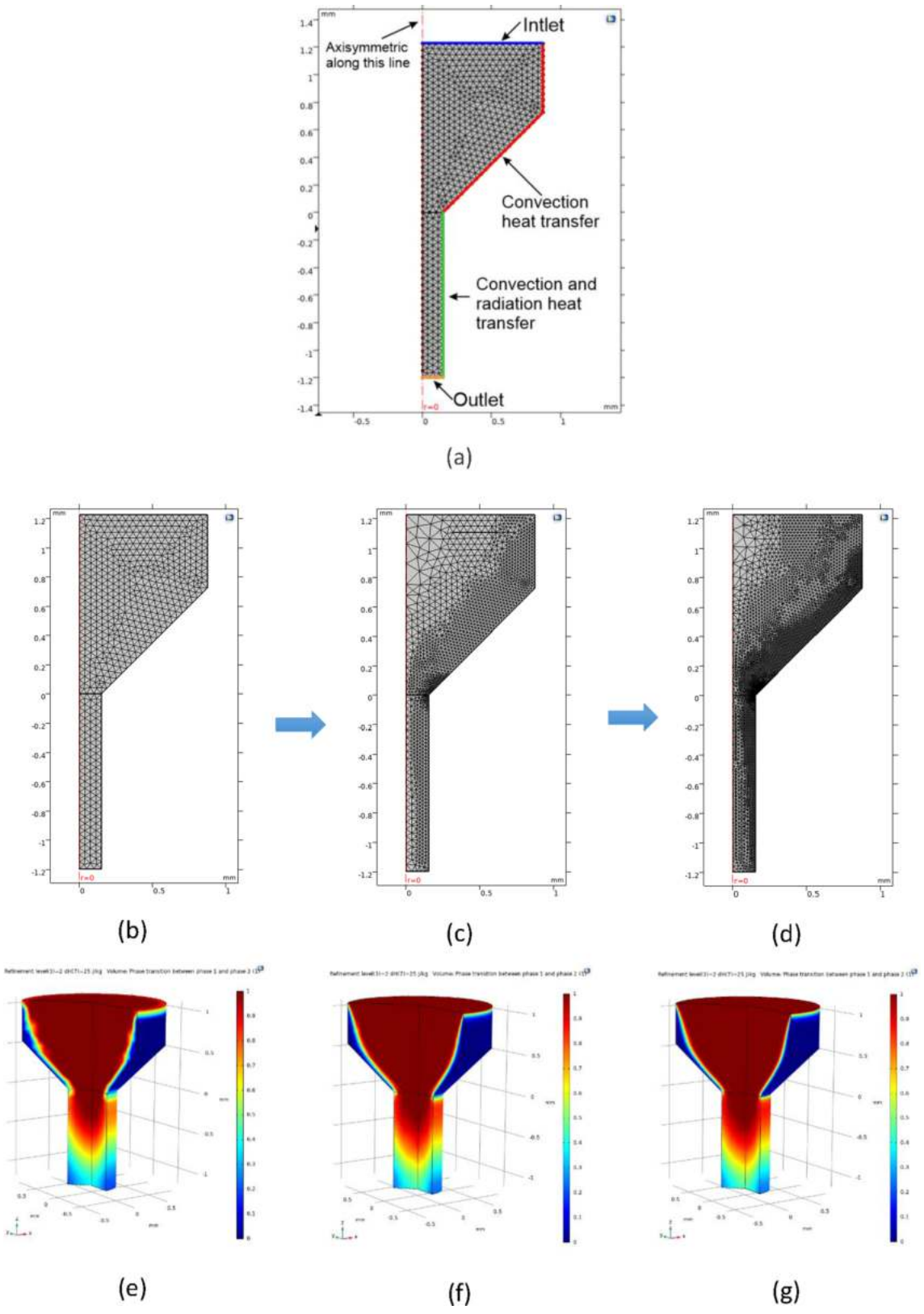

Fig. 5. FE simulation including: (a) boundary conditions for first step of meshing, (b-d) Adaptive mesh refinement in the extrusion process. (e-g) the results obtained from b-d meshing models, respectively.

can significantly improve the quality of bonding of the layers which can be achieved by keeping the temperature of the printed lines greater than its glass transition temperature [31,32]. The heat transfer process of the extruded polymer during the 3D printing process was determined experimentally using various techniques, for example, infrared thermography cameras [33–36]. Several experimental research studies have been conducted to define the heat transfer at the nozzle assembly [17,28,37]. During the 3D printing process of polymers, several heat

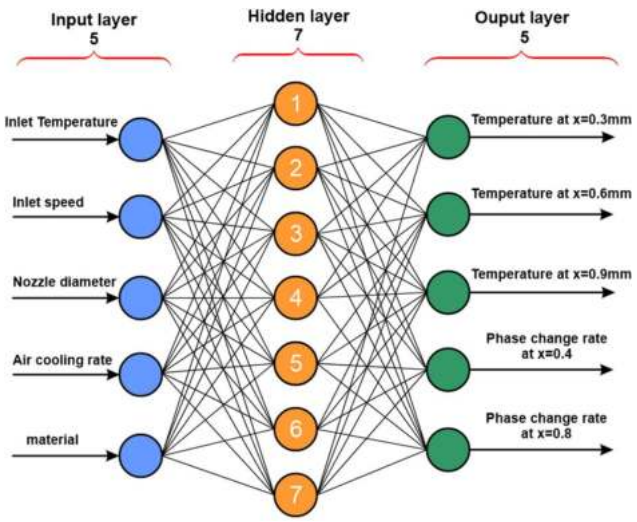

Fig. 6. The architecture of a trained ANN in this study.

transfer processes are present: radiation, convection, and phase change. All heat transfer processes significantly impact on the quality of the final 3D printed part. As such, the relative impact of these processing parameters needs to be determined. This requires high familiarity and accurate knowledge of the heat transfer process in the standoff region.

Unlike metals, the low thermal conductivity of polymers limits heating and cooling rates which results in shrinking and delamination during a cooling process [26]. Semi-crystalline polymers have a thermal conductivity higher than amorphous polymers. The structure of crystals in the polymer and consequently the physical properties of the semi-crystalline polymers are dependent on the rate of heat transfer during the cooling process [38]. A high percentage of large crystals are formed in polymer during their slow cooling process which remarkably increases on its hardness [27]. The 3D printing process is progressive, where a 3D model is built layer by layer. During this process, the deposited and solidified layer or layers experience a heating effect, due to subsequent layer(s), which influence the polymer's crystallinity. This leads to uneven cooling and reheating processes which can introduce residual stresses and as such, a reduction in the mechanical properties of the 3D printed model. Prajapati et al. [34] observed that in FDM models with thin walls, the extrusion temperature influences the extent of cracking and wrapping in the final model.

FE simulation is extensively used as a prediction tool to evaluate the cause and effect of the quality of deposited parts [22,39,40]. Thermo-mechanical analysis of FDM process was conducted by Courter et al. [41] using FE simulation and the effect of tool path on the residual stresses of the part of the model was investigated. Courter et al. [41] conducted an FEA study in which the thermal properties of materials including thermal expansion coefficient and conductivity were considered constant with only the specific heat capacity of polymer being a function of temperature. Zhou et al. [41] observed that there is desirable interaction between the tool path and the thermos-mechanical properties of the 3D printed parts. Although good agreement between the realistic and FEA results were observed, Zhou et al. [41] suggested that it is necessary to define all the thermal properties of polymers as a function of temperature and crystallinity. FE simulation and theoretical modelling of heat transfer and rheology of Poly lactic acid (PLA) polymer in the nozzle were carried out by Go et al. [30] and Phan et al. [42]. Go et al. [30] and Phan et al. [42] defined the thermal expansion coefficient as a function of temperature at two phases and reported the heat transfer between the PLA polymer and nozzle wall affect the overall printing quality. Zhou et al. [43] developed a 3D finite element model for thermal simulation of the FDM 3D printing process using birth-and-death feature. Zhou et al. [43] validated the model using the infrared thermography imaging method. Their results show a 13% difference between the numerical and experimental models. Zhou et al. [43] concluded such discrepancy is due to inaccurate modelling of the build plate heat transfer coefficient. Zhou et al. [43] also stated that the model with the build plate temperature set at the highest level might require further consideration. Improvement in the modified model can be used for the prediction of thermal behavior. Using continuous media theory, a thermal finite element simulation of the FDM 3D printing process of ABS materials was developed by Zhou et al. [44] and the results showed by changing the thermal properties of the material, the modelling method would significantly influence the thermal evaluation.

Several research studies have reported on the characterization and optimization of the 3D printing processing parameters [45–50]. For ABS polymer, the effect of layer height, layer width and extrusion speed on surface roughness of the FDM 3D printed parts was studied by Anitha et al. [45]. The obtained results revealed that the effect of layer height is most significant [45]. A derived relation was used as a cost function for optimization [43]. To optimize the surface roughness of the FDM 3D printed parts, Thrimurthulu et al. [46] developed an analytical model using the genetic algorithm to predict the orientation of the 3D model regardless of the complexity of the 3D model [51–53]. Four processing parameters, including the printing speed at two different sections of the model, layer height and layer width were considered by Zhang et al. [47]. The relation between these parameters and the accuracy and deformation of the FDM 3D printed parts were established using fuzzy comprehensive evaluation and Taguchi method and the optimum processing parameters were determined. A statistical optimization method was used by Wang et al. [48] to find the optimum processing parameters to optimize the surface roughness of the FDM 3D printed parts. A mathematical model was developed by Thrimurthulu et al. [46] to optimize the printing time. Thrimurthulu et al. [42] established the build orientation as the effective processing parameter and the optimum build orientation was determined using the genetic algorithm.

Artificial Neural Networks (ANNs) have been increasingly used as non-parametric predictors for solving complex problems [54]. Some researchers have used ANN to predict part quality in nonconventional and conventional machining process such as milling and drilling [55–57]. Their ANN results demonstrated that there is a close correlation between the processing parameters and the quality of the manufactured part. The processing parameters of numerous conventional manufacturing technologies can be calibrated during 3D printing process. While, adjusting some of the processing parameters such as printing pattern, printing orientation, layer thickness, nozzle diameter and shell thickness during the operation is unmanageable during the FDM 3D printing process [58]. Therefore, to train an ANN, the off-line approach is chosen as a function of some processing parameters. Researches have not thoroughly studied the combined effect of processing parameters and their correlation with the final quality of the FDM 3D printed parts [59–61]. The deficiency of a design method, especially in FE, and the lack of a reliable prediction technique might be the reason for many associated problems. Systematically conducted robust FE, analytical methods as well as a trustworthy prediction methods are currently lacking.

The aim of this study is to evaluate the significance of the combined effect of processing parameters using developed FE simulation analysis and an ANN Prediction Algorithm followed by experimental validation of the numerical results. The numerical and experimental results in this research contribute to the investigation and prediction of the phase change zones and thermal behavior of ABS and PA12 polymers the standoff region. To address the main objective of the study, a 3D transient finite element model was developed by integration of an apparent heat capacity method and adaptive mesh refinement method. Due to variation of thermal material properties of polymer by temperature, to achieve accurate numerical results, the thermal material properties of polymer were defined as a function of polymer temperature. The FE simulation was conducted using the Heat Transfer Module in COMSOL®

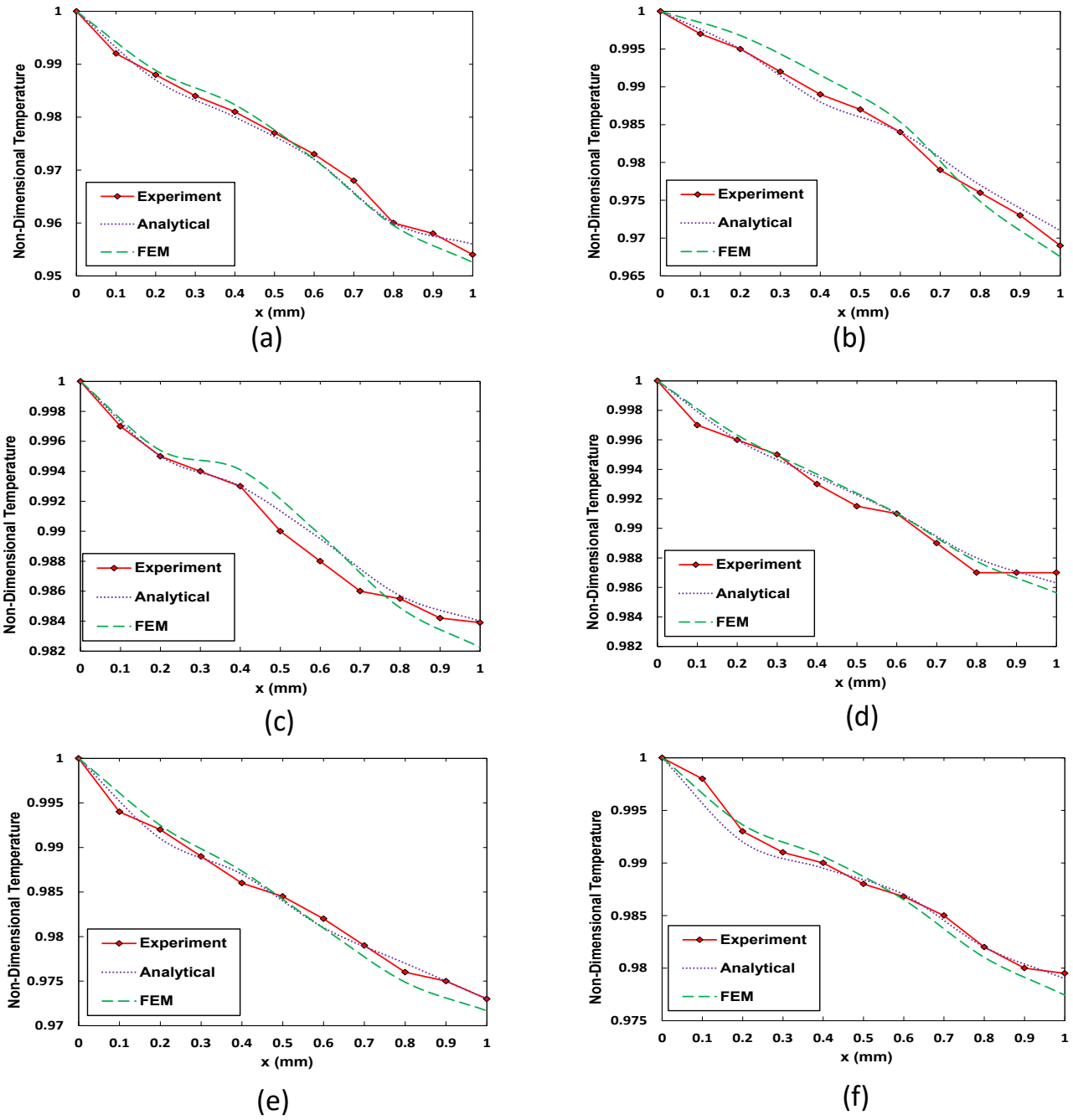

Fig. 7. Comparison of FE simulation associated with the thermal behavior of polymer in the distance between the build plate and nozzle tip: (a) Nozzle size 0.4 mm and speed 4.5 mm/s, (b) Nozzle size 0.4 mm and speed 7.5 mm/s, (c) Nozzle size 0.4 mm and speed 16.5 mm/s, (d) Nozzle size 0.4 mm and speed 20 mm/s, (e) Nozzle size 0.6 mm and speed 6 mm/s, (f) Nozzle size 0.6 mm and speed 8 mm/s.

Multiphysics software package. The FE simulation results were then validated by the experiment results. The influence of several processing parameters including: nozzle size, extrusion, and air cooling speed on the glass transition and thermal behavior of polymers was numerically studied. The FE simulation results were used to train an ANN for predicting and optimizing the processing parameters of the FDM 3D printing.

This paper is structured as follows: experimental procedure to determine the temperature distribution of the extruded polymer at the distance between nozzle tip and build plate is presented in section 2 and section 3. In Section 4, the mathematical formulation of heat transfer in the distance between the nozzle tip and build plate is presented. In Section 5, thermal material properties of polymers, including: thermal conductivity, heat capacity, and density are defined as a function of temperature and the finite element modelling of the extrusion process in the standoff region is discussed. Section 6 refers to the application of ANN in the prediction of glass transition and thermal behavior of polymer in the distance between the nozzle tip and build plate. ANN training is based on the FE simulation results. Finally, the FE simulation and ANN results are discussed in Section 7.

2. Experimental apparatus and test procedures:

To determine the temperature distribution of extruded polymer at the standoff region, an infrared thermal camera was used. To provide a reliable optical access to the distance between the nozzle tip and build

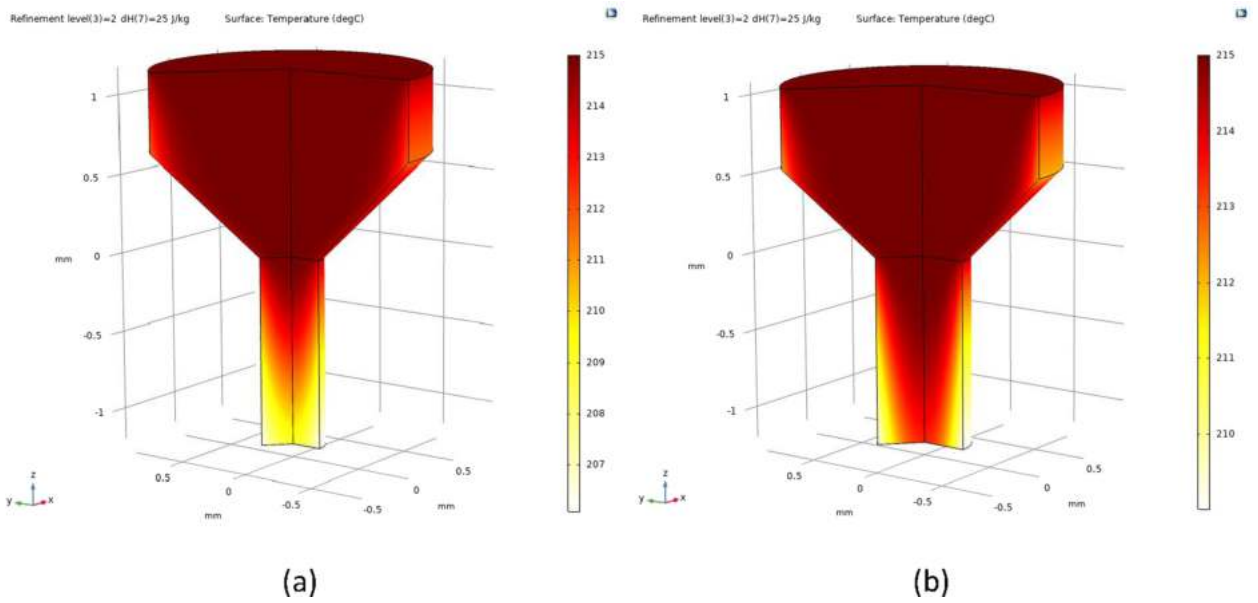

Fig. 8. The temperature distribution of ABS polymer in the distance between the nozzle tip and build plate: (a) Nozzle size 0.4 mm and speed 6 mm/s, (b) Nozzle size 0.6 mm and speed 8 mm/s.

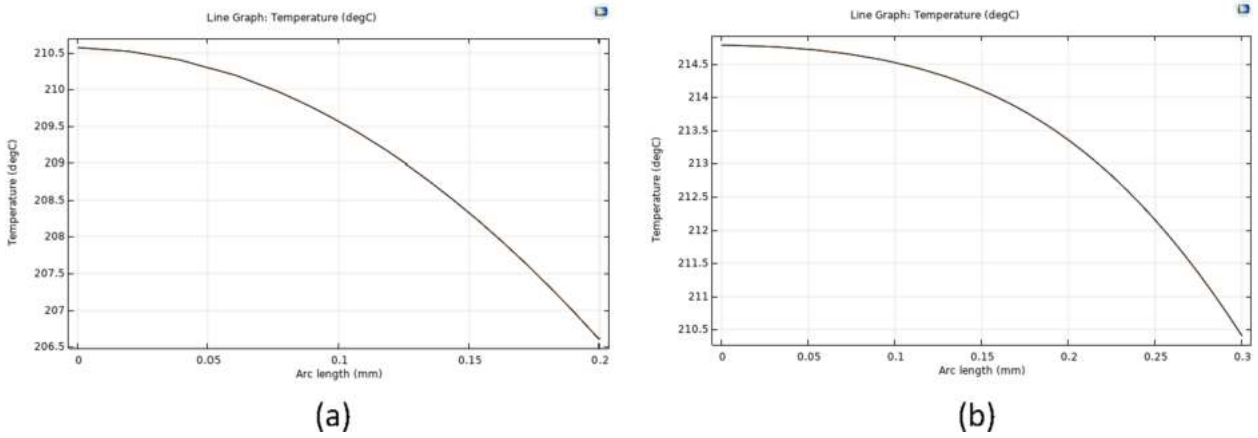

Fig. 9. the variation of temperature in the transverse direction and within the cross-section of extruded polymer: (a) Nozzle size 0.4 mm and speed 6 mm/s, (b) Nozzle size 0.6 mm and speed 8 mm/s.

plate, custom-made polymer extrusion system encompasses a set of E3D hotend (including: exchangeable nozzle, heater, Heater block, NTC100K thermistor, nozzle barrel and heat sink), filament feeder (including stepper motor, gear, and ball bearing) and an Arduino Mega 2560 and ramps 1.6 based motherboard with stepper driver of DRV8850 was designed and used for accurate extrusion of polymer. Fig. 2 illustrates a schematic of design extrusion system and infrared thermal camera.

3. Experimental results and discussion

Upon accurate calibration of extrusion system, using ABS polymer and two different sizes of brass nozzle (0.4 mm and 0.6 mm), five experiments were conducted at different extrusion speeds and the temperature distribution along the standoff region (up to $\times = 1$ mm from the tip of the brass nozzle) were recorded. The obtained results are presented in Fig. 3, which shows that in the standoff region, the highest and the lowest temperature variations occur when the polymer is extruded using a nozzle size of 0.4 mm at an extrusion speed of 4.4 mm/s and 20.2 mm/s, respectively. The extrusion speed has a significant influence on temperature variation within the standoff region for both nozzle sizes 0.4 mm and 0.6 mm. Increasing the extrusion speed results in the extruded polymer losing less energy, i.e. increase the extrusion speed, decrease the temperature variation in the standoff region.

4. Mathematical modelling

In the extrusion process, as illustrated in (Fig. 1a), the melted polymer with a mass flow of $\dot{m}$ leaves the nozzle tip ($x = 0$) and deposits on the build plate ($x = L$). As polymer is extruded from the nozzle tip, two types of heat transfers including radiation and convection occurs at the distance between the nozzle tip and build plate. For simplification purpose, it was assumed that the temperature distribution of polymer in this region is steady-state; and, the temperature of the build plate does not have any effect on the thermal behavior of the extruded polymer.

Using the mathematical relationship in (Fig. 1b) and considering the thermal material properties of polymer and two types of heat transfers, the total energy balance of an element of length dx can be derived as per Eq.1 [62]:

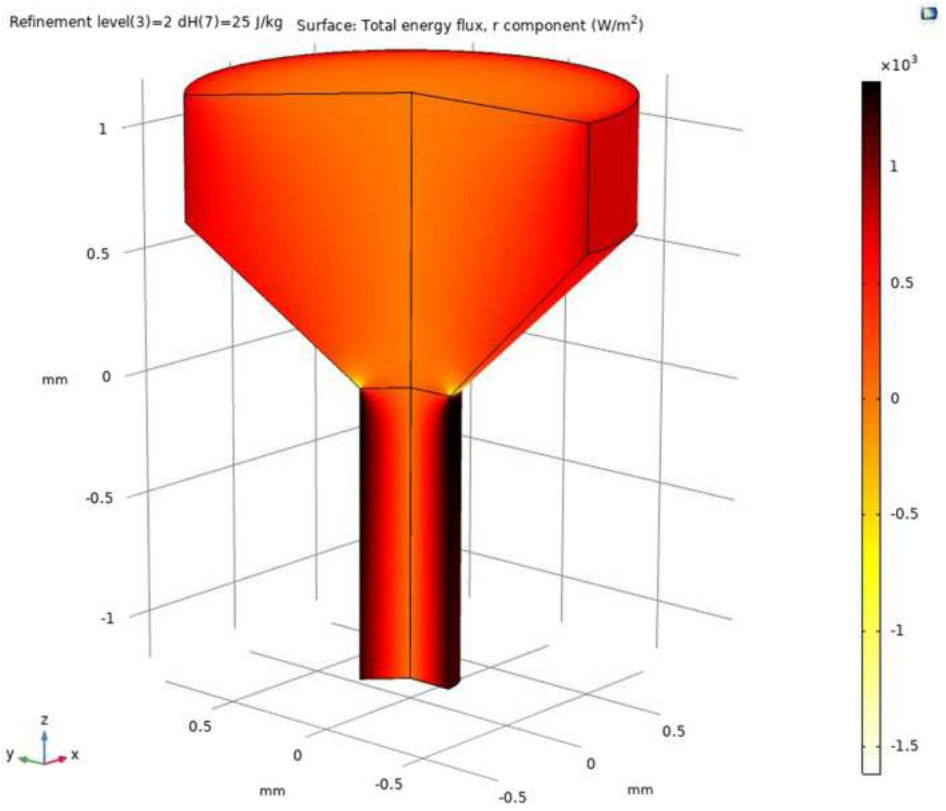

Fig. 10. The overall energy flux of molten ABS polymer during the extrusion process.

$$\dot{m}C_pT = \dot{m}C_p\left(T + \frac{dT}{dx}dx\right) + h_c(T - T_{am})Pdx + \in \sigma\left(T^4 - T_r^4\right)Pdx \tag{1}$$

where, P, $\dot{m}$ and C_p stand for the diameter of extruded polymer, mass flow rate, and the heat capacity of polymer, respectively. T_{am}, $\in$, σ and h_c are the ambient temperature, emissivity of polymer, Stefan-Boltzmann constant, and convective heat transfer coefficient, respectively.

The total energy balance equation (Eq.1) can be defined in a brief format as per Eq.2 [62]:

$$\frac{dT}{dx} = -\frac{h_cP}{\dot{m}C_p}(T - T_{\text{am}}) - \frac{\in \sigma P}{\dot{m}C_p}\left(T^4 - T_r^4\right) \tag{2}$$

Due to the non-linearity of Eq.2, defining an analytical solution is very challenging. The numerical simulation of Eq.2 can be derived by linearizing the radiative term through writing an estimated radiative heat transfer coefficient, h_r (Eq.3) [62]:

$$h_r = \in \sigma\left(T_{eff}^2 + T_r^2\right)\left(T_{eff} + T_r\right) \tag{3}$$

The effective temperature of polymer (T_{eff}) can be estimated by average temperature of extruded polymer which can be calculated using Eq.4:

$$\frac{dT}{dx} = -\frac{h_{eff}P}{\dot{m}C_p}(T - T_\infty) h_{eff} = h_c + h_\infty \tag{4}$$

Eq.5 is used to calculate the temperature distribution in polymer:

$$\theta = \frac{T - T_\infty}{T_0 - T_\infty} = exp\left(-\frac{x}{x_0}\right)x_0 = \frac{\dot{m}C_p}{h_{eff}P} \tag{5}$$

Based on Eq.5, the temperature of polymer reduces nonlinearly along the extrusion direction [16].

Using fluid dynamic and thermal analysis, the conduction behavior of polymer were defined by Rahman et al. [63]. Other processing parameters in the polymer extrusion process including: the nozzle size, air cooling, printing speed, and melt flow and glass transition regions should be considered when developing an accurate model [63].

Heat transfer is then derived based on the assumption in [60] as Eq.6:

$$\rho C_p u.\nabla T + \nabla.(-k\nabla T) = Q \tag{6}$$

where,C_p, Q, k, and u are the specific heat capacity of polymer, heat power per volume unit, thermal conductivity, and extrusion speed in two states, respectively. After polymer is extruded from the nozzle, it cools to its glass transition state and releases a large amount of energy. Considering the changes in heat capacity and enthalpy, the amount of energy per unit mass can be calculated using Eq.7 which is based on the variation of the specific heat capacity [63]:

$$\Delta C_p = \frac{\Delta H}{T} \tag{7}$$

To relate the heat to glass transition of polymer, an apparent heat capacity method is used for the heat transfer with a phase change domain [64,65]. The aim of this analysis is to define ΔT and by considering that the flow is laminar, the fluid velocity (u) and pressure (p) are stated in Eqs.8,9 [63]:

$$\rho\frac{\partial u}{\partial t} + \rho u.\nabla u = \nabla.\left[-pI + \mu(\nabla u) + (\nabla u)^T - \left(\frac{2\mu}{3} - \kappa\right)(\nabla.u)I\right] + F \tag{8}$$

$$\frac{\partial \rho}{\partial t} + \nabla.(\rho u) = 0 \tag{9}$$

where, κ and μ represent the dilatational viscosity and viscosity of polymer, respectively. The term F is the dampen of the velocity of polymer at the modulus-change interface, which can be calculated using Eq.10 [63]:

$$F = \frac{(1-\alpha)^2}{\alpha^3 + \varepsilon}A_m(u - u_{ex}) \tag{10}$$

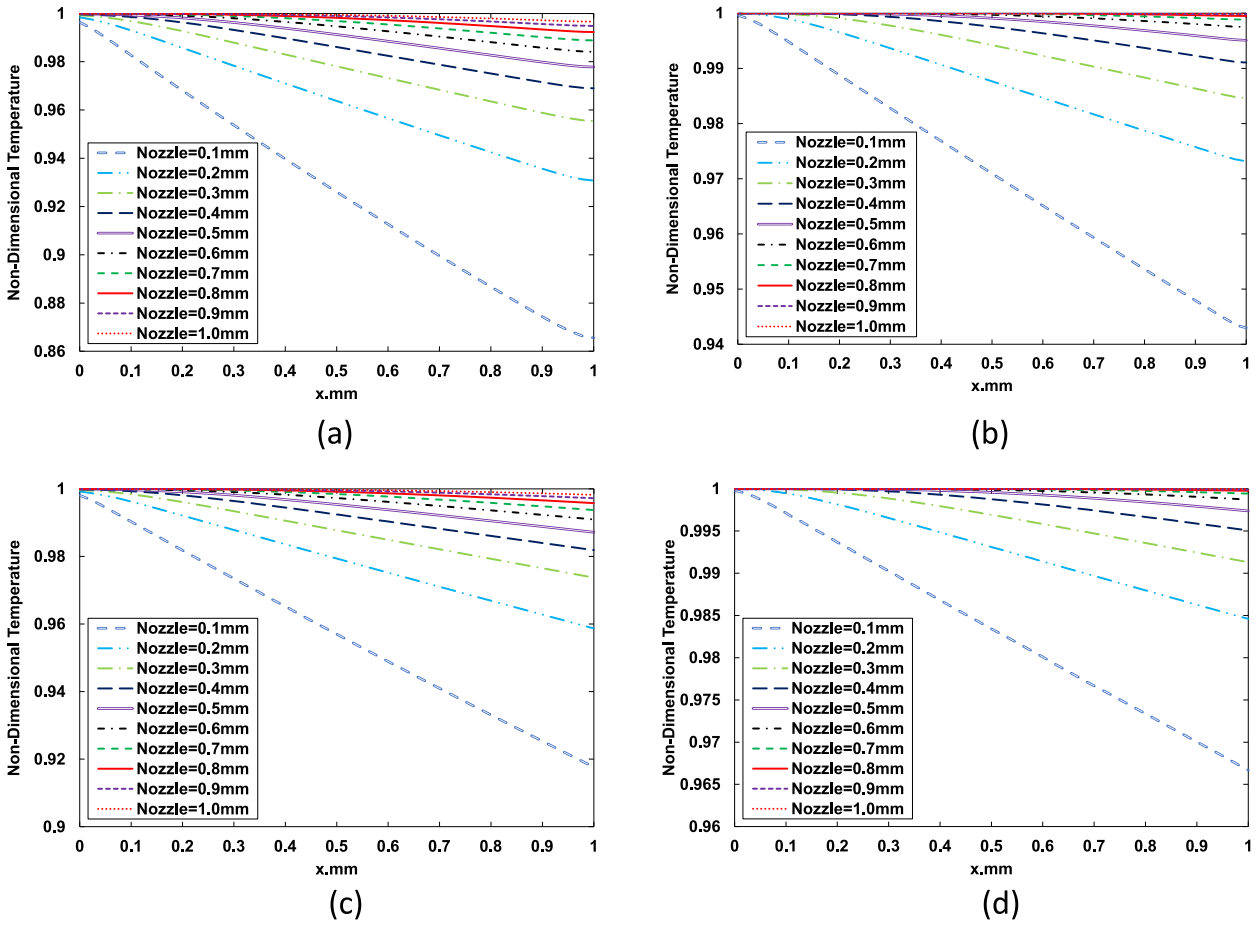

Fig. 11. Thermal behavior of ABS and PA12 Polymers at the distance between the nozzle tip and build plate: (a) ABS polymer (speed 4 mm/s), (b) ABS polymer (speed 10 mm/s), (c) PA12 polymer (speed 4 mm/s), (d) PA12 polymer (speed 10 mm/s).

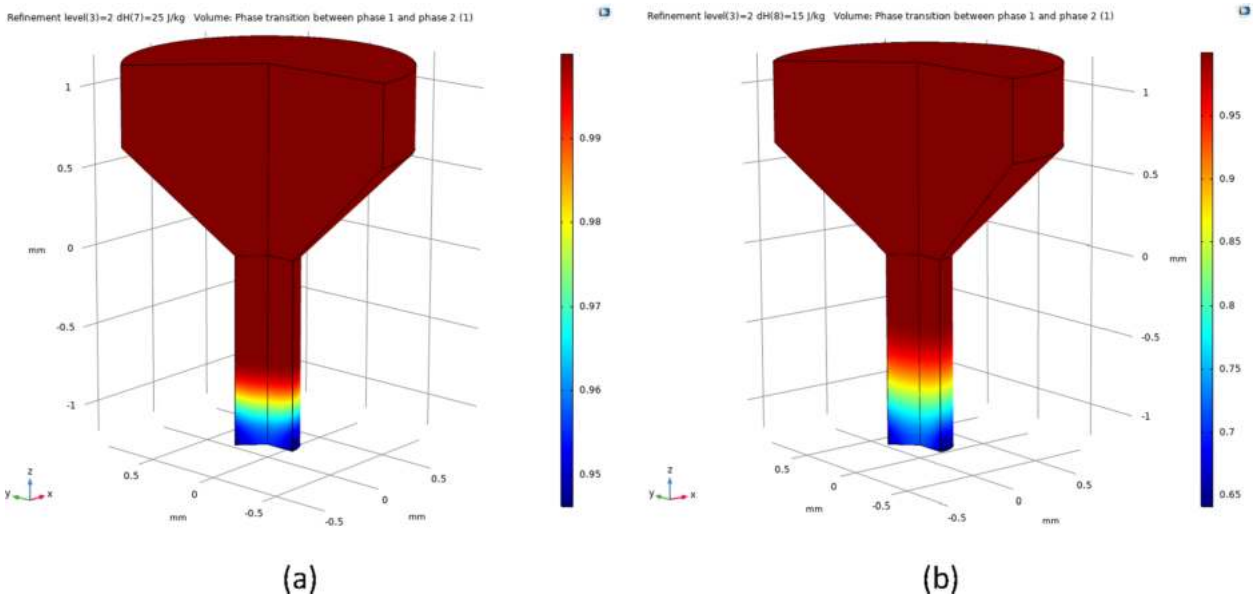

Fig. 12. The glass transition behavior of polymers using a nozzle with diameter 0.4 mm: (a) ABS polymer at speed 0.15 mm/s, (b) PA12 polymer at speed 0.26 mm/s.

Where, u_{ex}, α, ε and A_m are the velocity, volume fraction of the liquid phase and arbitrary constants, respectively [28].

The glass transition behavior of polymers in the FDM 3D printing process is nonlinear and it is a function of various processing parameters such as temperature, air cooling and extrusion speed. Therefore, a converged mesh in the phase change zones should be employed to assess accurate results.

Table 2
The inlet speed of polymer in extrusion system at a constant outlet speed of 4 mm/s.

Nozzle size (mm)	0.1	0.2	0.3	0.35	0.4	0.5	0.6	0.7	0.8	0.9	1.0
Inlet velocity (mm/s)	0.0131	0.052	0.117	0.16	0.209	0.326	0.47	0.64	0836	1.06	1.31

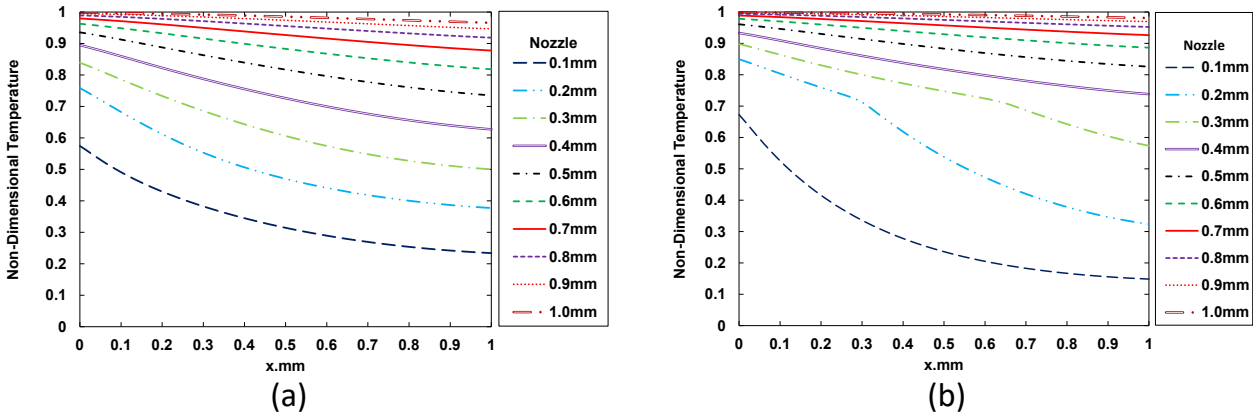

Fig. 13. The effect of nozzle size on non-dimensional temperature of the polymer at the distance between the nozzle tip and build plate: (a) ABS polymer, (b) PA12 polymer.

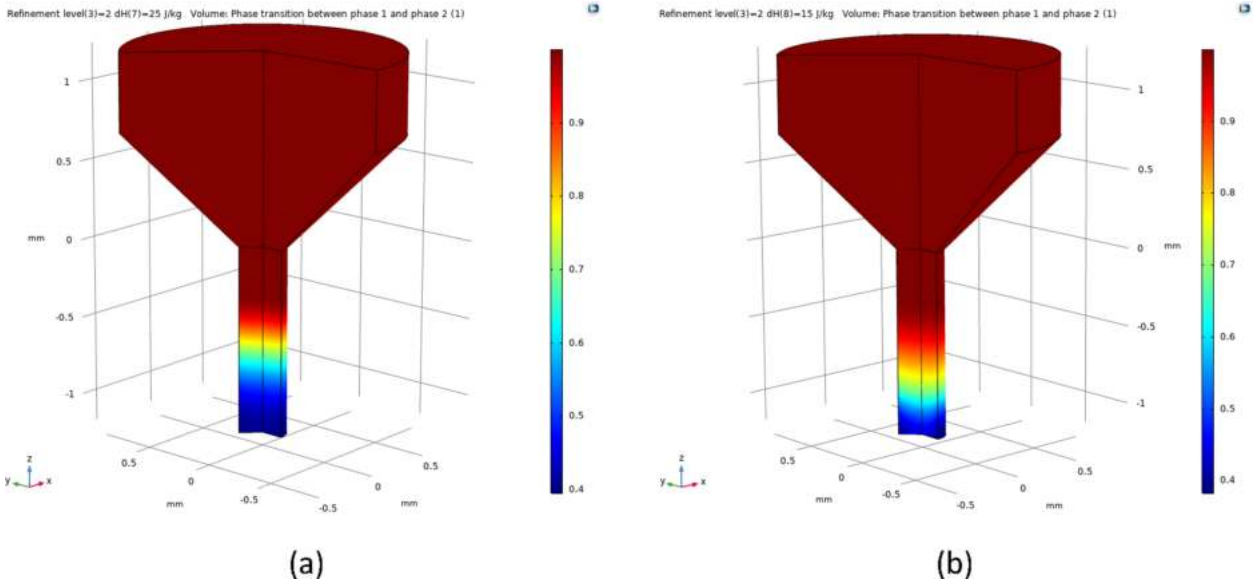

Fig. 14. The glass transition behavior of ABS and PA12 polymers using a nozzle with diameter of 0.3 mm at extrusion speed of 0.117 mm/s and air-cooling speed of 15 m/s: (a) ABS polymer, (b) PA12 polymer.

5. Finite element simulation:

5.1. Material modeling

The thermal properties of the polymer including the glass transition temperature, the melting temperature, the heat capacity and the thermal conductivity have considerable effect on the overall quality of 3D printed [66]. The melting temperature of semi-crystalline polymers occurs at a sharp point, while amorphous polymers do not have a specific melting temperature. In other words, they are high viscos in the melt state which results in no flowability since the viscosity is reduced by increasing the temperature [67]. Therefore, the peak of the differential scanning calorimetry (DSC) curve is assumed to be the melting temperature of amorphous polymer[68].

In this study, the Polyamide 12, PA12 (PA2200, EOS GmbH) as a semi-crystalline polymer [69] and Acrylonitrile Butadiene Styrene (ABS) as an amorphous polymer [3] selected and their thermal material properties including the temperature-dependent heat capacity, heat conductivity and density of polymers were obtained from the literature [63,70,71] which is illustrated in Fig. 4. The melting and solidification temperature of PA12 polymer is at 169.7 °*C* and 154.2 ℃, respectively [70]. The thermal conductivity, density and specific heat capacity of ABS and PA12 polymers in both glassy and rubbery states at constant pressure are listed in Table.1 [63].

5.2. Finite element modeling

To simulate the polymer phase change, the Heat Transfer Module in COMSOL® Multiphysics software package (based on an apparent heat capacity method) was used. This Module is suitable for various phase

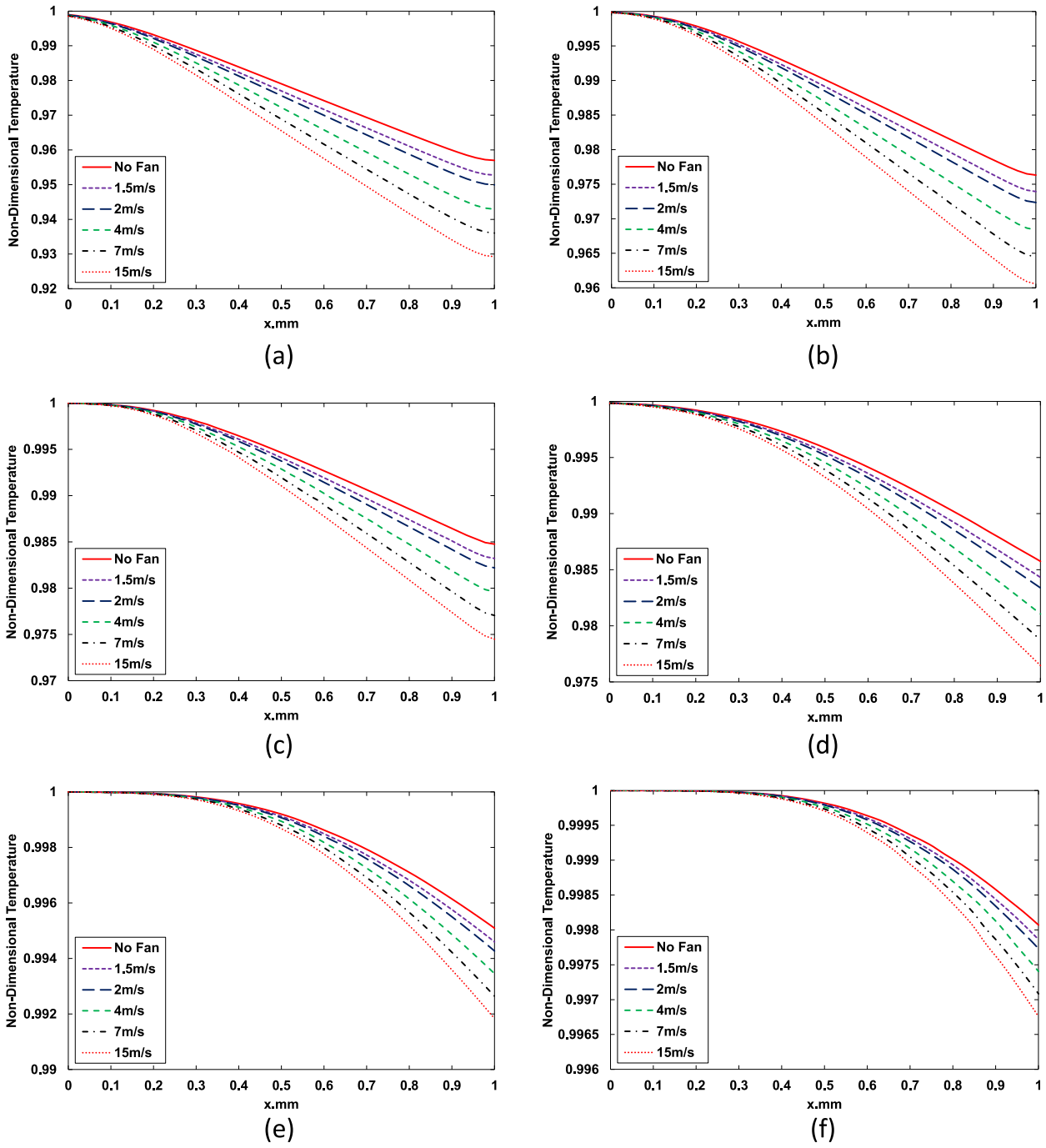

Fig. 15. Thermal behavior of ABS polymer at the distance between the build plate and nozzle tip at different setup: (a) Nozzle size 0.4 mm and speed 3 mm/s, (b) Nozzle size 0.4 mm and speed 5 mm/s, (c) Nozzle size 0.4 mm and speed 7 mm/s, (d) Nozzle size 0.8 mm and speed 3 mm/s, (e) Nozzle size 0.8 mm and speed 5 mm/s, (f) Nozzle size 0.8 mm and speed 7 mm/s.

transitions [72,73]. To use this COMSOL® Module for accurate modelling of phase change between the solid and liquid states, the thermal material properties of polymer should be defined separately for both states as a function of temperature and phase transition function $\alpha(T)$. Properties include the heat capacity, thermal conductivity, and density of polymer. The phase transition function is equal to zero and one for a pure solid and a pure liquid, respectively [60]. In the FE simulation, 2D axisymmetric models, due to the extrusion system's axial symmetry, were used. Parameters that significantly affect the location of transition between the glassy and rubbery states include: extrusion speed, cooling speed, nozzle size and extrusion temperature (Section 1). Therefore, it is necessary to use fine mesh across the transition state to consider the effect of temperature-dependent material properties. A continuous adaptive mesh refinement algorithm in COMSOL® was used to find the solidification region. Based on this algorithm, the simulation is initiated by a gradual transition between the glassy and rubbery states using coarser mesh in first stage. The first simulation was then used as a starting point for the next step of simulation with a finer mesh, and this process was repeated until the best convergence was achieved. In the present study, the linear trial mesh was used for meshing the model. The boundary condition for the first step of meshing is illustrated in (Fig. 5a and Fig. 5b-g), and demonstrates the adaptive mesh refinement method. The boundary conditions in (Fig. 5a) are similarly adopted for the next steps of meshing model.

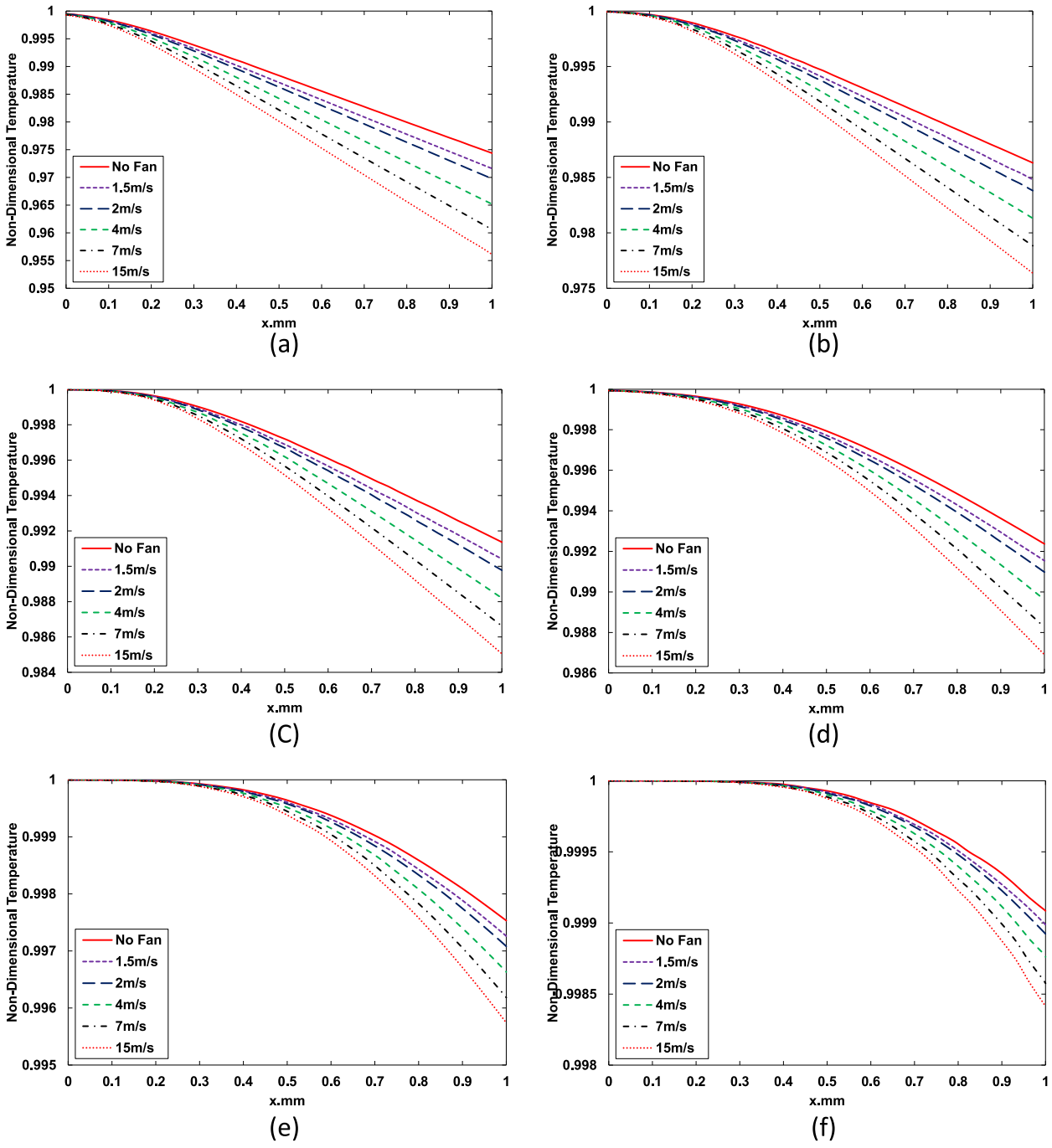

Fig. 16. Thermal behavior of PA12 polymer at the distance between the build plate and nozzle tip at different setup: (a) Nozzle size 0.4 mm and speed 3 mm/s, (b) Nozzle size 0.4 mm and speed 5 mm/s, (c) Nozzle size 0.4 mm and speed 7 mm/s, (d) Nozzle size 0.8 mm and speed 3 mm/s, (e) Nozzle size 0.8 mm and speed 5 mm/s, (f) Nozzle size 0.8 mm and speed 7 mm/s.

6. The artificial neural network approach:

Artificial neural networks (ANNs) are non-parametric predictors that offer useful and viable means for solving complex problems and for solution predictions [54]. ANNs can predict hidden functional relationships between the effective processing parameters and polymer phase change or thermal behavior of the extrusion system as inputs and output of networks, respectively [74]. ANNs were developed to mimic the biological nervous system [75,76]. The nodes or neurons, weights and connections (dendrites and synapses) are the main components of ANNs. A set of input and out data should be used to train an ANN. Once the training of an ANN is done, the ANN can then be used to estimate other input data that has not been used during the training process. This capability is called generalization [77,78].

ANNs consist of four steps including the definition of input and outputs, setting database, designing, and training the network and evaluation. The aim of using ANNs in this study is to determine the temperature and phase change rate in the extrusion process. A set of effective processing parameters as discussed before including the inlet temperature and speed, nozzle diameter, cooling rate and type of material are ANN input parameters. The temperature and phase change rate at different points along the distance between the nozzle tip and build plate are as output ANN parameters. A set of the normalized database

consists of 98 finite element models were analyzed and used in

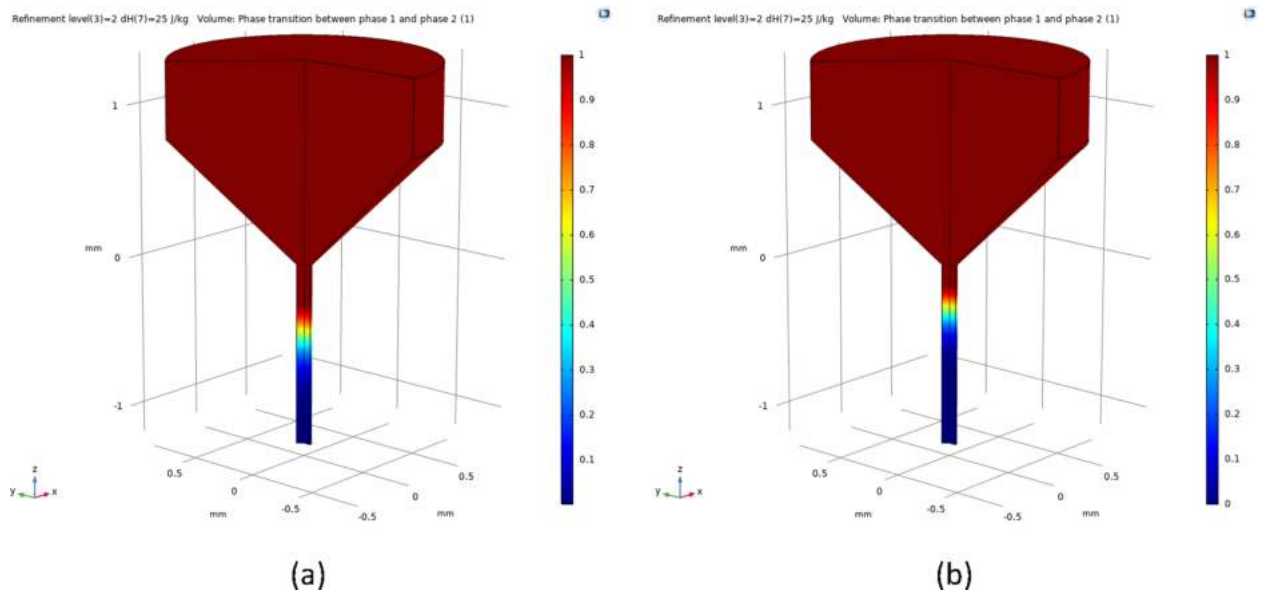

Fig. 17. The phase change behavior of ABS polymer at two air-cooling speeds including (a) 1.5 m/s, (b) 7 m/s.

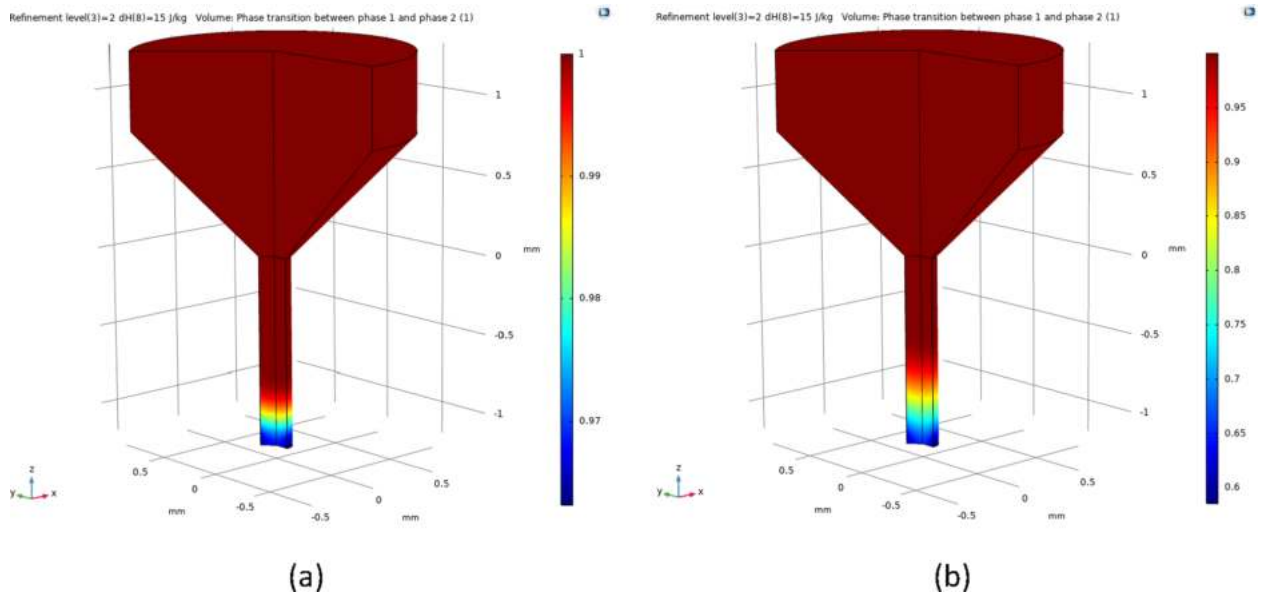

Fig. 18. The two-phase transition between the liquid and solid phases of PA12 polymer extrusion at two different air-cooling speeds: (a) 1.5 m/s and (b) 7 m/s.

training different architecture of ANNs using the Levenberg-Marquardt [58,79–81] algorithm in MATLAB Software. From that normalized database, 80% of data was used for training the networks and 15% and 5% of data was used for validation and performance testing, respectively. After compiling the database, the integrity of data was checked using Microsoft Excel Spreadsheet to find the most effective parameters and eliminate the data which can make noise during the training process.

The performance of ANNs significantly depends on the architecture of the network. As such, there is no guideline for the choice of appropriate architecture. Trial and error experiments are normally used to assess the most-optimum ANN architecture. In this study, multilayer perceptron architecture using the Levenberg-Marquardt algorithm and trial and error method was used to test and find the optimum number of hidden layers for the ANN with highest performance. It has been observed that an ANN consists of one input layer with five neurons, one output layer with five neurons, and one hidden layer with seven neurons offers the highest performance for this study (Fig. 6).

The inlet temperature and speed, air cooling rate, types of materials and nozzle diameter were considered as input parameters for the ANN and the temperature and phase change rate at different points alongside the distance between the nozzle tip and build plate were assumed as output parameters (Fig. 6). The training process ended after 245 epochs with the mean error and validation set of 2.235e-6 and 4.857e-6, respectively.

7. Results and discussions

7.1. Validation of the FE simulation results

The FE simulation was carried out to determine the influence of four different inlet extrusion speeds 4.5 mm/s, 7.5 mm/s, 16.5 mm/s and 20 mm/s for the nozzle size 0.4 mm and two different inlet extrusion speeds 6 mm/s and 8 mm/s for nozzle size 0.6 mm. several points along the

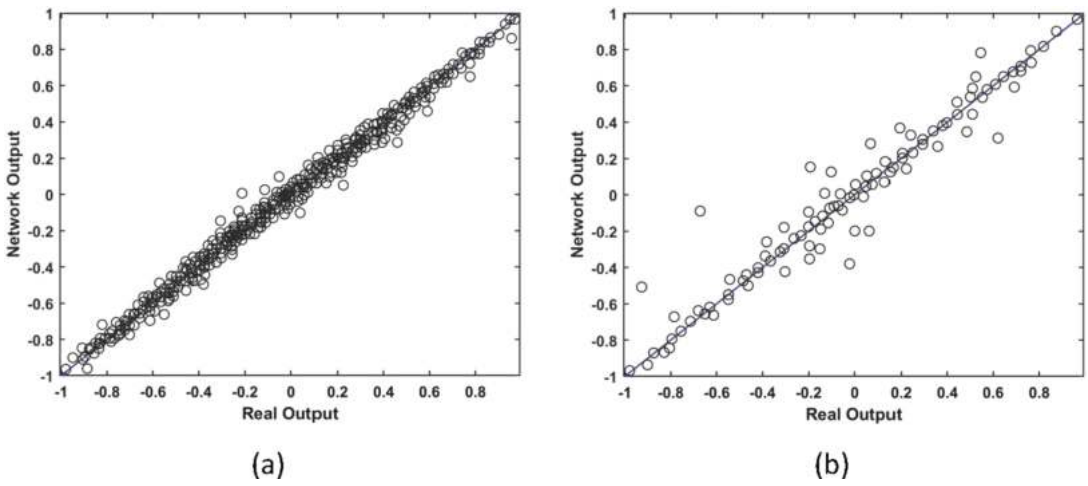

Fig. 19. Network output vs real output for (a) train data b) test data.

Table 3
Comparison between the FE simulation results and the predicted ANN results.

		Model 1	Model 2	Model 3	Model 4
Extrusion speed (mm/s)		4	5	6	10
Nozzle diameter (mm)		0.4	0.9	0.45	0.65
Air cooling speed (m/s)		10	0	5	0
Type of material		ABS	ABS	PA12	PA12
Inlet temperature (Celsius)		195	245	228	210
Non-Dimensional Temperature at x = 0.3 mm	**ANN:**	0.983	0.998	0.993	0.99
	FEA:	0.982	0.996	0.994	0.993
	Square Error (%):	0.0001	0.0004	0.0001	0.0009
Non-Dimensional Temperature at x = 0.6 mm	**ANN:**	0.953	0.99	0.985	0.99
	FEA:	0.953	0.991	0.985	0.989
	Square Error (%):	0	0.0001	0	0.0001
Non-Dimensional Temperature at x = 0.9 mm	**ANN:**	0.922	0.984	0.974	0.984
	FEA:	0.924	0.986	0.973	0.983
	Square Error (%):	0.0004	0.0004	0.0001	0.0001
Phase change rate at x = 0.4 mm	**ANN:**	0.998	1	0.999	0.998
	FEA:	1	1	1	1
	Square Error (%):	0.0004	0	0.0001	0.0004
Phase change rate at x = 0.8 mm	**ANN:**	0.983	0.993	0.991	0.995
	FEA:	0.985	0.994	0.993	0.994
	Square Error (%):	0.0004	0.0001	0.0004	0.0001

distance between the nozzle tip and build plate were identified and the temperature distribution at these points was compared with experiment results, and shown in Fig. 7. From the analytical and experiment results, it is observed that there is a nonlinear relationship between the temperature of extruded polymer and the extrusion speed. Temperature is dropped when the distance from nozzle tip and extrusion speed is increased.

Comparing the FE simulation, experimental, and analytical results (Fig. 7), it can be seen that FEM results of the temperature of the extruded polymer estimate slightly lower and higher, respectively, in the first and second half of the distance between the build plate and nozzle tip. Low-temperature prediction in the first half can be attributed to two assumptions: First, the nozzle surface is isolated and there is no heat transfer between the environment and the nozzle surface; second, the extruded polymer is fully circular, and its diameter is constant. In reality and according to die-swell theory [42], the cross-section of polymer in the distance between the nozzle tip and build plate changes slightly and there is some radiation and convection heat transfer between the surrounding environment and the nozzle surface.

Fig. 8 shows the temperature distribution of ABS polymer in the distance between the nozzle tip and build plate for nozzle sizes of 0.4 mm and 0.6 mm with extrusion speeds 6 mm/s and 8 mm/s, respectively. Fig. 9 shows the thermal behavior of ABS along the cross- section of extruded polymer for two different nozzle sizes of 0.4 mm and 0.6 mm with extrusion speeds 6 mm/s and 8 mm/s, respectively. It can be observed from Fig. 8 and Fig. 9 that the variation of temperature in the transverse direction and within the cross-section is minimal, about 2%, and these results are almost the same as the recorded temperature

through the experiment. Comparing the present FEM results with the experimental and analytical results, demonstrates a reliable agreement in the temperature results in x and transverse directions. Therefore, the developed finite element model can be employed to study the influence of the processing parameters on the temperature distribution of the polymer in the extrusion system.

The glass transition behavior of ABS polymer is evaluated at an extrusion temperature of 105 $^{\circ}C$. Using a nozzle with a diameter of 0.4 mm, the molten ABS polymer is extruded at a speed of 1 mm/s. In this study, the heat transfer (convection) between the surface of the nozzle and the surrounding environment (25 $^{\circ}C$) is considered. Fig. 10 shows the overall energy flux in the process, where the lowest and highest energy flux are released outside the nozzle and in the nozzle assembly, respectively. The energy flux is reduced with distance from the nozzle center. A small amount of energy flux is released at the nozzle tip due the released heat in the secondary glass transition once the molten polymer is extruded through the nozzle.

7.2. *Nozzle size:*

Using the FE simulation, the thermal behavior of two types of polymers including ABS and PA12 polymers at the extrusion temperature of 215 $^{\circ}C$ were studied. The effect of nozzle size on temperature distribution at two constant speeds (4 mm/s and 10 mm/s) and the ambient temperature of 25 $^{\circ}C$, were analysed and the results are illustrated in Fig. 11.

In this section, the effect of inlet speed was studied without considering the impact of nozzle diameter on outlet speed. It can be seen from Fig. 11 that at a constant inlet extrusion speed, the nozzle size significantly affects temperature distribution in the polymer. The temperature is reduced by increasing the nozzle size. Next, the increasing the size of the nozzle from 0.2 mm to 0.6 mm at a constant speed of 4 mm/s will increase the temperature of ABS polymer and PA12 polymer at $x = 0.5mm$ by 3.2% and 1.84%, respectively. In other words, the effect of nozzle size in the amorphous polymer (ABS) is higher than the semi-crystalline polymer (PA12). By increasing the size of the nozzle, the

heat transfer (convention) from the outer surface of the extruded polymer is increased. In contrast, the temperature in the polymer's center-line is changed slightly because the cooling rate is higher on the outer surface. According to physics laws (the equation of continuity), increasing the diameter of the nozzle at a constant inlet speed reduces the outlet speed which consequently influences the temperature distribution of the extruded polymer. Comparing the obtained results for the temperature distribution of ABS polymer at two different extrusion speeds (4 mm/s and 6 mm/s), indicated that the extrusion speed slightly affects the center-line temperature. For an example, in extrusion process of ABS polymer through two nozzle sizes of 0.5 mm and 0.8 mm, increasing the speed from 4 mm/s to 10 mm/s increases the temperature at $\times = 0.5$ mm by 0.8% and 0.15%, respectively.

To study the glass transition behavior of polymer during the extrusion process, the extrusion process of ABS and PA12 polymers were simulated at the same extrusion temperature (215 $^{\circ}C$) with various extrusion speeds as well as the effect of nozzle size on glass transition behavior. It was observed that no glass transition occurs in the distance between the nozzle tip and build plate for both polymers. Under respective extrusion conditions, the polymer remains liquid at the distance between the build plate and nozzle tip. It was noticed that the extrusion speed and temperature will affect the location of the glass transition. For instance, the glass transition takes place in the distance between the build plate and nozzle if the extrusion speed of ABS polymer is set to lower than 0.65 mm/s and 0.3 mm/s for nozzle size of 0.2 mm and 0.4 mm, respectively. At the same conditions, the extrusion speed for PA12 polymer should be lower than 1.1 mm/s and 0.56 mm/s, respectively. As illustrated in Fig. 12, the glass transition of ABS and PA12 polymers using a nozzle with a diameter of 0.4 mm occurs at the distance between the nozzle tip and build plate if the extrusion speed is set to 0.15 mm/s and 0.26 mm/s, respectively.

In practice, during the 3D printing process, the extrusion speed depends on the printing speed. For optimization and better control of the overall quality of the 3D printed model, it is crucial to have a thorough understanding of the nozzle effects on temperature distribution and glass transition behavior of polymer at a constant speed and flow rate. The outlet extrusion speed was kept constant at 4 mm/s, and the inlet extrusion speed for different size of nozzle was calculated using a physics law which states that the volume flow rate at a nozzle is constant, and it is a function of cross-section and the speed of flow ($Q = A_i v_i = A_o v_o$). Using volume flow rate law at a constant outlet speed or polymer, the inlet speed of polymer is calculated and listed in Table.2.

Next, the influence of nozzle diameter on glass transition and thermal behavior of two types of polymers including PA12 and ABS polymers were studied numerically at a constant extrusion temperature of 215 $^{\circ}C$, ambient temperature of 25 $^{\circ}C$ and various inlet speed as listed in Table 2. The obtained results are illustrated in Fig. 13.

For both types of polymers, by keeping the outlet extrusion speed as a constant value, it can be seen from Fig. 13 that the diameter of the nozzle significantly affects the temperature distribution in the distance between the nozzle tip and build plate. By increasing the diameter of the nozzle from 0.2 mm to 0.6 mm, the temperature of the polymer at $\times = 0.5$ mm is increased by 88.2% and 73.5%, respectively. A large release of energy in the small nozzles causes a complete phase change in mentioned distance. A typical example is, for nozzle size of 0.3 mm, the glass transition of ABS is occurred near the nozzle tip, and for PA12, it is taken place far from the tip of the nozzle, as seen in Fig. 14.

7.3. Air- cooling speed:

To study the effect of air-cooling speed on the glass transition behavior and temperature distribution of extruded ABS and PA12 Polymers, two sets of nozzles including 0.4 mm and 0.8 mm were selected and the extrusion process of these polymers at different extrusion speeds 3 mm/s, 5 mm/s and 7 mm/s were simulated using developed FE. The extrusion temperature (215 $^{\circ}C$) and the ambient temperature (25 $^{\circ}C$) were kept constant in all simulations. The obtained results at different air-cooling speeds for ABS and PA12 are illustrated in Figs. 15 and 16, respectively.

Fig. 15 and Fig. 16 show that the effect of air-cooling on the temperature of the extruded for ABS and PA12 polymers is lower than other processing parameters due to the short distance between the build plate and nozzle tip. For instance, by adding an air-cooling process at the speed of 7 m/s to an extrusion process using two sets of the nozzle including 0.4 mm and 0.8 mm, the temperature of the extruded polymer at the middle of the distance between the nozzle tip and build plate is reduced by 0.5% and 0.05%, respectively. As mentioned in Subsection 6.1, cooling processes are mainly occurred on the outer surface of the extruded polymer. The temperature variation between the outer surface and the middle are 1.2% and 1%, respectively. Comparing graphs (a) and (c) in Fig. 15 shows that the effect of air-cooling speed on the thermal behavior of the extruded ABS polymer at higher speed is lower because, increasing the extrusion speed reduces the heat transfer's duration in the mentioned region. For instance, adding an air-cooling system at speed of 15 m/s to an extrusion process of PA12 polymer using two sets of nozzles including 0.8 mm and 0.4 mm at the extrusion speed of 3 mm/s, reduces the temperature of the extruded polymer at the middle of the distance by 0.15% and 0.85%, respectively. Comparing the obtained results for both types of the polymers at different air-cooling rates showed that the effect of the air-cooling process on the temperature of the semi-crystalline polymer (PA12) is higher than the amorphous polymer (ABS) which should be assumed to set the processing parameters.

The phase change between the solid and liquid states in the extrusion process of ABS and PA12 polymers at two different air-cooling speeds including 1.5 m/s and 7 m/s using a nozzle size of 0.1 mm and extrusion speed of 1 mm/s are illustrated in Fig. 17 and Fig. 18, respectively. In this study, the extrusion processing parameters were chosen as the phase change appears in the distance between the nozzle tip and build plate. Comparing the obtained results, showed that the air-cooling process affects slightly on the location of phase change in the distance between the nozzle tip and build plate. The polymer phase is changed at air-cooling speed of 1.5 m/s is appeared at a distance of 0.35 mm from the nozzle tip. By increasing the air-cooling speed to 7 m/s, the location of phase change is appeared at the distance of 0.23 mm from the nozzle tip, which is closer to nozzle tip.

7.4. Prediction of temperature distribution and phase change rate:

As mentioned in Section 5, Five processing parameters, including the nozzle diameter (0.1 mm to 1 mm), air cooling rate (0 to 15 m/s), type of material (ABS, PA12), inlet temperature (180 $^{\circ}C$ to 250 $^{\circ}C$) and extrusion speed (3 mm/s to 10 mm/s) were set as inputs (Section 5). The glass transition rate from rubbery state to solid-state and temperature at different points along the distance between the nozzle tip and build plate were set as outputs. The inputs and outputs were then used to train the network. (Fig. 19a and 19b) demonstrate the plot of network output vs real data for train data and test data of temperature and phase change rate at different places along the distance between the nozzle tip and build plate, respectively. As illustrated in the figures, the errors are low, and the output data is satisfactorily dispersed. This indicates that the ANN is readily able to predict temperature and phase change rates. It can be also observed that the randomness of data was assured.

The accuracy of the trained ANN model and comparison its result with FE simulation results were also investigated using the four new models which have not been used in the earlier network training processes. Each model contains different processing parameters, as shown in Table 3. It can be seen in Table 3 that there is a close agreement between the predicted results using trained ANN and FE results. For instance, for ABS material at an extrusion speed of 5 mm/s and air temperature of 245 $^{\circ}C$, nozzle diameter of 0.9 mm without any air-cooling process, the square error between the ANN and FE results at

× = 0.6 mm is 0.1%. The maximum difference between the ANN and FE results is 0.3% for temperature and 0.2% for phase change rate. Due to the number of various processing parameters and interaction among them, the setting suitable processing parameters to successfully achieve 3D printing process is required.

The processing parameters are manually adjusted by user in most of the slicing software in the FDM 3D printing technology. For those users who cannot access to FE for analyzing the effect of adjusted parameters on the quality of 3D printed models, the trained ANN can be integrated with a software slicing engine. In other words, implemented slicing software can predict the thermal behavior of selected polymer based on the user defined parameters to suitably define processing parameters. Such integration can guide FDM 3D printer users in smart processing parameters selection and regulation. This procedure can be then alternatively used in order to predict the temperature distribution and phase change rate of polymer extrusion process in the 3D printing process.

8. Conclusions

The present study investigated the influence of the FDM 3D printing processing parameters, the inlet and outlet extrusion speeds, nozzle size, and cooling rate, on the thermal and phase change behavior of ABS and PA12 polymers. The analysis focused on the distance between the nozzle tip and build plate in the FDM extrusion process using the steady state FE simulation based on an apparent heat capacity method in COMSOL® Multiphysics software. The FE simulation results were compared with, and validated by, a series of the experiments. The FE simulation results were also used to train an ANN for further prediction. The FE simulation results indicated that the thermal behavior of polymer and the

phase change rate of polymer in the distance between the nozzle tip and build plate (standoff region) are influenced by extrusion processing parameters. It was found that the nozzle size is one of the most effective processing parameters in the FDM 3D printing process. The temperature of extruded polymer in the distance between the nozzle tip and build plate was reduced by increasing the nozzle size, which effects the amorphous polymer (ABS) far more than the semi-crystalline polymer (PA12). Furthermore, it was observed that the extrusion speed effects the glass transition zone along the distance between the nozzle tip and build plate and the center-line temperature. Due to the short distance between the build plate and nozzle tip, air cooling rate on the temperature of the extruded polymers is lower than that of other processing parameters and its effect on the temperature of the semi-crystalline polymer (PA12) is higher than that of the amorphous polymer (ABS).

The comparison of the numerical and experimental results showed good agreement which demonstrates that FE simulation can be employed to train an ANN. In addition, the trained ANN can be adopted to further predict the phase change rate and thermal distribution of polymers at the distance between the nozzle tip and build plate. Both FE simulation and ANN methods are reliable and robust methods and can be used to optimize the processing parameters in the FDM 3D printing. This study also demonstrated that a trained ANN can be used as an alternative to FE.

Declaration of Competing Interest

The authors declare that they have no known competing financial interests or personal relationships that could have appeared to influence the work reported in this paper.

Acknowledgements

N.M would like to acknowledge the funding received from UTM under the Post-Doctoral Fellowship Scheme (Grant. No. Q. J130000.21A2.05E30) for the Project: “Uniaxial and Biaxial Ratcheting of a Girth-Welded Super Duplex Stainless Steel (UNS S32750) Pressurized Pipe”.

References:

[1] Apparatus for production of three-dimensional objects by stereolithography, (August 1984).
[2] J.S.H. Emanuel M. Sachs, Michael J. Cima, Paul A. Williams, Three-dimensional printing techniques, US Patent, 5,204,055 (1993).
[3] P. Wang, B. Zou, S. Ding, Modeling of surface roughness based on heat transfer considering diffusion among deposition filaments for FDM 3D printing heat-resistant resin, Appl. Therm. Eng. 161 (2019), 114064.
[4] I. Gibson, D. Rosen, B. Stucker (Eds.), Additive Manufacturing Technologies, Springer New York, New York, NY, 2015.
[5] R.S.G.D.T. Pham, A comparison of rapid prototyping technologies, Int. J. Mach. Tool Manufact 38 (1998) 1257–1287.
[6] W.E. Frazier, Metal additive manufacturing: a review, J. Mater. Eng. Perform 23 (6) (2014) 1917–1928.
[7] M.C.L.J.P. Kruth, T. Nakagawa, Progress in additive manufacturing and rapid prototyping, CIRP Ann. 47 (1998) 525–540.
[8] V.H.G.J.P. Vojislav, J.F. Olga, D.G. Javier, R.B.P. Jose, P.G. Luis, Additive layered manufacturing: sectors of industrial application shown through case studies, Int. J. Prod. Res 49 (2010) 1061–1079.
[9] N. Li, S. Huang, G. Zhang, R. Qin, W. Liu, H. Xiong, G. Shi, J. Blackburn, Progress in additive manufacturing on new materials: a review, J. Mater. Sci. Technol. 35 (2) (2019) 242–269.
[10] L.E. Murr, Frontiers of 3D Printing/Additive Manufacturing: from Human Organs to Aircraft Fabrication, J. Mater. Sci. Technol. 32 (2016) 987–995.
[11] A. Haleem, M. Javaid, 3D printed medical parts with different materials using additive manufacturing, Clinical Epidemiology and Global, Health 8 (1) (2020) 215–223.
[12] A. Bhardwaj, S.Z. Jones, N. Kalantar, Z. Pei, J. Vickers, T. Wangler, P. Zavattieri, N. Zou, Additive Manufacturing Processes for Infrastructure Construction: a Review. Proceedings of the ASME 2019 14th International Manufacturing Science and Engineering Conference. Volume 1: Additive Manufacturing; Manufacturing Equipment and Systems; Bio and Sustainable Manufacturing, 2019.
[13] A.B. Davin Jankovics, D. Jankovics, A. Barari, Customization of Automotive Structural Components using Additive Manufacturing and Topology Optimization, IFAC-PapersOnLine 52 (2019) 212–217.
[14] F.F. Ramdhani, B. Mulyanti, Additive manufacturing in education, IOP Conf. Series, Materials Science and Engineering 830 (4) (2020) 042093.
[15] G.R. Manish Kamal, Design for metal additive manufacturing for aerospace applications, (2019) 67-86.
[16] H. Bikas, P. Stavropoulos, G. Chryssolouris, Additive manufacturing methods and modelling approaches: a critical review, Int J Adv Manuf Technol 83 (1-4) (2016) 389–405.
[17] M.E. Mackay, Z.R. Swain, C.R. Banbury, D.D. Phan, D.A. Edwards, The performance of the hot end in a plasticating 3D printer, J. Rheol 61 (2) (2017) 229–236.
[18] A. Jaisingh Sheoran, H. Kumar, Fused Deposition modeling process parameters optimization and effect on mechanical properties and part quality: review and reflection on present research, Mater. Today:. Proc. 21 (2020) 1659–1672.
[19] C. Abeykoon, P. Sri-Amphorn, A. Fernando, Anura Fernando, Optimization of fused deposition modeling parameters for improved PLA and ABS 3D printed structures, International Journal of Lightweight Materials and Manufacture 3 (3) (2020) 284–297.
[20] S. Wang, Y. Ma, Z. Deng, S. Zhang, J. Cai, Effects of fused deposition modeling process parameters on tensile, dynamic mechanical properties of 3D printed polylactic acid materials, Polym. Test. 86 (2020).
[21] T.N.H.V.H. Nguyen, T.P. Nguyen, T.T. Tran, Single and Multi-objective Optimization of Processing Parameters for Fused Deposition Modeling in 3D Printing Technology, international journal of automotive and mechancial engineering 17 (2020) 7542–7551.
[22] S.K.P. Ashutosh Pandey, Investigations into Complete Liquefier Dynamics and Optimization of Process Parameters for Fused Deposition Modeling, Mater. Today:. Proc. 5 (2018) 301–307.
[23] S.H.M.O.A. Mohamed, J.L. Bhowmik, Optimization of fused deposition modeling process parameters: a review of current research and future prospects, J. Adv. Manuf. 3 (2015) 42–53.
[24] N.Y.A. Dey, A systematic survey of FDM process parameter optimization and their influence on part characteristics, J. Manuf. Mater. Processing 3 (2019) 64.
[25] S.M.M. Moradi, A. Kaplan, 3D printed parts with honeycomb internal pattern by fused deposition modelling; experimental characterization and production optimization, Met. Mater. Int. 25 (2019) 312–1325.
[26] C. Rauwendaal, Polymer extrusion, Hanser Publishers, München, 2001.
[27] G.R. Stroble, The Physics of Polymers, Springer, Berlin, 1997.
[28] B.D.V.F. Peng, M. Cakmak, Complex flow and temperature history during melt extrusion in material extrusion additive manufacturing, Addit. Manuf 22 (2018) 197–206.
[29] S.G.A. Bellini, M. Bertoldi, Liquefier dynamics in fused deposition, J. Manuf. Sci. Eng 126 (2007) 237–246.
[30] A.J.H.J. Go, Fast desktop-scale extrusion additive manufacturing, Addit. Manuf 18 (2017) 276–284.
[31] B.G. Compton, B.K. Post, C.E. Duty, L. Love, V. Kunc, Thermal analysis of additive manufacturing of large-scale thermoplastic polymer composites, Addit. Manuf. 17 (2017) 77–86.
[32] F.M.D.S.F. Costa, J.A. Covas, Estimation of filament temperature and adhesion development in fused deposition techniques, J. Mater. Process. Technol 245 (2017) 167–179.

[33] D.W.D. Anthony, D. Wetz, A. Jain, Non-invasive measurement of internal temperature of a cylindrical Li-ion cell during high-rate discharge, Int. J. Heat Mass Tran 111 (2017) 223–231.
[34] Y.A.L. Dupont, P. Jeannin, Comparison of junction temperature evaluations in a power IGBT module using an IR camera and three thermosensitive electrical parameters, Int. J. Heat Mass Tran 49 (2013) 1599–1608.
[35] H.F. Hamann, A. Weger, J.A. Lacey, Z. Hu, P. Bose, E. Cohen, J. Wakil, Hot spot limited microprocessors: direct temperature and power distribution measurements, IEEE J. Solid State Circ 42 (1) (2007) 56–65.
[36] M.S. Carvalho, A.P. Martins, T.G. Santos, Simulation and validation of thermography inspection for components produced by additive manufacturing, Appl. Therm. Eng. 159 (2019), 113872.
[37] M.Y.L.J.H. Park, S.Y. Kwon, H.J. Roh, M.S. Koo, S.H. Cho, Temperature analysis of nozzle in a FDM type 3D printer through computer simulation and experiment, Elastomers Compos 51 (2016) 301–307.
[38] D.H. Morton-Jones, Polymer Processing, Chapman and Hall, 1992.
[39] Y. Zhang, Y.K. Chou, Three-dimensional finite element analysis simulations of the fused deposition modelling process, Proceedings of the Institution of Mechanical Engineers, Part B: Journal of Engineering Manufacture 220 (10) (2006) 1663–1671.
[40] Y. Zhang, K. Chou, A parametric study of part distortions in fused deposition modelling using three-dimensional finite element analysis, Proceedings of the Institution of Mechanical Engineers, Part B: Journal of Engineering Manufacture. 222 (8) (2008) 959–968.
[41] V.S.B. Courter, J. Bi, S. Dev, C.J. Hansen, Finite element simulation of the fused deposition modelling process, Proceedings of the NAFEMS World Congress (2017) 11–14.
[42] D.D. Phan, Z.R. Swain, M.E. Mackay, Rheological and heat transfer effects in fused filament fabrication, J. Rheol 62 (5) (2018) 1097–1107.
[43] X.Z.S.-J. Hsieh, Thermal analysis of fused deposition modeling process using infrared thermography imaging and finite element modeling, Proc. SPIE 10214, Thermosense: Thermal Infrared Applications XXXIX, (2017) 1021409.
[44] T.N.Y. Zhou, G. Xiong, D. Liu, Temperature Analysis in the Fused Deposition Modeling Process, 3rd International Conference on Information Science and Control Engineering (ICISCE), Beijing, China, 2016.
[45] T.R.D.R.V. Nancharaiah, D.R. Raju, V.R. Raju, An experimental investigation on surface quality and dimensional accuracy of FDM components, International Journal on Emerging Technologies 1 (2) (2010) 106–111.
[46] K.P.P.M. Thrimurthulu, P.M. Pandey, N.V. Reddy, Optimum part deposition orientation in fused deposition modeling, Int. J. Mach. Tools Manuf 44 (6) (2004) 585–594.
[47] A.H.P.J.W. Zhang, Process-parameter optimization for fused deposition modeling based on Taguchi method, Adv Mater Res 538 (2012) 444–447.
[48] T.W.L. C. C. Wang, S. S. Hu Optimizing the rapid prototyping process by integrating the Taguchi method with the gray relational analysis, Rapid Prototyp J, 13 (2007) 304-315.
[49] G.F.C.H.Y. Wan, C.P. Li, X.B. Qi, G.P. Zhang, Data-driven evaluation of fatigue performance of additive manufactured parts using miniature specimens, J. Mater. Sci. Technol. 35 (2019) 1137–1146.
[50] Q.S. Ruishan Xie, G. Chen, Improved distortion prediction in additive manufacturing using an experimental-based stress relaxation model, J. Mater. Sci. Technol. 59 (2020) 83–91.
[51] M.G.Z.N. Moslemi, A. Ayob, N. Redzuan, S. Rhee, Evaluation of sensitivity and calibration of the chaboche kinematic hardening model parameters for numerical ratcheting simulation, Applied Sciences 9 (2019) 2578.
[52] N. Moslemi, M. Golzardian, N. Redzuan, F. Mozafari, A. Ayob, Optimization procedure for parameter determination of caboche kinematic hardening model, IOP Conference Series: Materials Science and Engineering 884 (1) (2020) 012112.
[53] F.M. N Moslemi*, B Abdi, S Gohari, N Redzuan*, C Burvill, A Ayob, Uniaxial and biaxial ratcheting behavior of pressurized AISI 316L pipe under cyclic loading: Experiment and simulation, N Moslemi, F Mozafari, B Abdi, S Gohari, N Redzuan*, C Burvill, A Ayob, 179 (2020) 105693.
[54] S. Motahar, M. Jahangiri, Transient heat transfer analysis of a phase change material heat sink using experimental data and artificial neural network, Appl. Therm. Eng. 167 (2020), 114817.
[55] H. El-Mounayri, J.F. Briceno, M. Gadallah, A new artificial neural network approach to modeling ball-end milling, The International Journal of Advanced Manufacturing Technology 47 (5) (2010) 527–534.
[56] J. Balic, Neural-network based numerical control milling machine, J Intell Robot Syst 40 (2004) 343–358.
[57] P. Muñoz-Escalona, P.G. Maropoulos, Artificial neural networks for surface roughness prediction when face milling Al 7075–T7351, J. Mater. Eng. Perform. 19 (2) (2010) 185–193.
[58] V.G.A. Boschetto, F. Veniali, Surface roughness prediction in fused deposition modelling by neural networks, Int J Adv Manuf Technol 67 (2013) 2727–2742.
[59] R.V. Pazhamannil, P. Govindan, P. Sooraj, Prediction of the tensile strength of polylactic acid fused deposition models using artificial neural network technique, Materials Today: Proceedings, in press 46 (2021) 9187–9193.
[60] K.P.M.K.V. Dhinakaran, P.M. Bupathi Ram, M. Ravichandran, M. Vinayagamoorthy, A review on recent advancements in fused deposition modeling, Mater. Today:. Proc. 27 (2020) 752–756.
[61] S. Vyavahare, S. Teraiya, D. Panghal, S. Kumar, Fused deposition modelling: a review, Rapid Prototyping Journal 26 (1) (2020) 176–201.
[62] D.R.H. Prajapati, A. Jain, Measurement and modeling of filament temperature distribution in the standoff gap between nozzle and bed in polymer-based additive manufacturing, Addit. Manuf. 24 (2018) 224–231.
[63] N.R.S. Miftahur Rahman, L.K. Sadhu, Glass Transition of ABS in 3D Printing. Excerpt from the Proceedings of the 2016 COMSOL Conference in Boston, 2016.
[64] H.M. Ali, Analysis of heat pipe-aided graphene-oxide based nanoparticle-enhanced phase change material heat sink for passive cooling of electronic components, J. Therm. Anal. Calorim. 146 (2021) 277–286.
[65] F. Hassan, F. Jamil, A. Hussain, H.M. Ali, M.M. Janjua, S. Khushnood, M. Farhan, K. Altaf, Z. Said, C. Li, Recent advancements in latent heat phase change materials and their applications for thermal energy storage and buildings: a state of the art review, Sustainable Energy Technol. Assess. 49 (2022), 101646.
[66] T.D. J.Brady, P.I.Lee, J.-X.Li, Chapter 7 - Polymer Properties and Characterization, Pharmaceutical Theory and Practice, (20017) 181-223.
[67] K.R.M. Lori, R. Hilden, Physics of amorphous solids, Physics of amorphous solids 93 (2004) 3–12.
[68] C. Schick, Differential scanning calorimetry (DSC) of semicrystalline polymers, Anal. Bioanal. Chem. 395 (6) (2009) 1589–1611.
[69] M. Ali, R.K. Sari, U. Sajjad, M. Sultan, H.M. Ali, Effect of annealing on microstructures and mechanical properties of PA-12 lattice structures proceeded by multi jet fusion technology, Addit. Manuf. 47 (2021), 102285.
[70] M.D.D. Riedlbauer, D. Drummer, P. Steinmann, J. Mergheim, Modelling, simulation and experimental validation of heat transfer in selective laser melting of the polymeric material PA12, Comput. Mater. Sci. 93 (2014) 239–248.
[71] R.S. Ranvijay Kumar, I. Farina, On the 3D printing of recycled ABS, PLA and HIPS thermoplastics for structural applications, PSU Research Review 2 (2014) 115.
[72] S. Mazloum, S. Awad, N. Allam, Y. Aboumsallem, K. Loubar, M. Tazerout, Khaled Loubar, Mohand Tazerout, Modelling plastic heating and melting in a semi-batch pyrolysis reactor, Appl. Energy 283 (2021) 116375.
[73] A. Ejaz, F. Jamil, H.M. Ali, A novel thermal regulation of photovoltaic panels through phase change materials with metallic foam-based system and a concise comparison: An experimental study, Sustainable Energy Technologies and Assessments, 49 (2022) 101726.
[74] S.H. Huang, H.-C. Zhang, Artificial neural networks in manufacturing: concepts, applications, and perspectives, IEEE Trans. Compon. Packag. Manuf. Technol. Part A: 17 (1994) 212–228.
[75] W. Wu, W. Deng, Y. Huang, X. Wang, Y. Ji, Prediction of the working conditions for the pulse tube cooler based on artificial neural network model, Appl. Therm. Eng. 197 (2021), 117424.
[76] K. Zhang, Z. Zhang, Y. Han, Y. Gu, Q. Qiu, X. Zhu, Artificial neural network modeling for steam ejector design, Appl. Therm. Eng. 204 (2022), 117939.
[77] J. Munguía, J. Ciurana, C. Riba, Neural-network-based model for build-time estimation in selective laser sintering, Proceedings of the Institution of Mechanical Engineers, Part B: Journal of Engineering Manufacture 223 (8) (2009) 995–1003.
[78] P. Gupta, P. Kumar, S.M. Rao, Artificial neural network model for single-phase real gas ejectors, Appl. Therm. Eng. 201 (2022), 117615.
[79] E.P. Oliveira, G.d.M. Stieven, E.F. Lins, J.R. Vaz, An inverse approach for the interfacial heat transfer parameters in alloys solidification, Applied thermal engineering, 155 (2019) 365-372.
[80] C.-H. Huang, Y.-T. Wu, An optimum design for a natural convection pin fin array with orientation consideration, Appl. Therm. Eng. 188 (2021), 116633.
[81] A. Fguiri, C. Marvillet, M.R. Jeday, Estimation of fouling resistance in a phosphoric acid/steam heat exchanger using inverse method, Appl. Therm. Eng. 192 (2021), 116935.